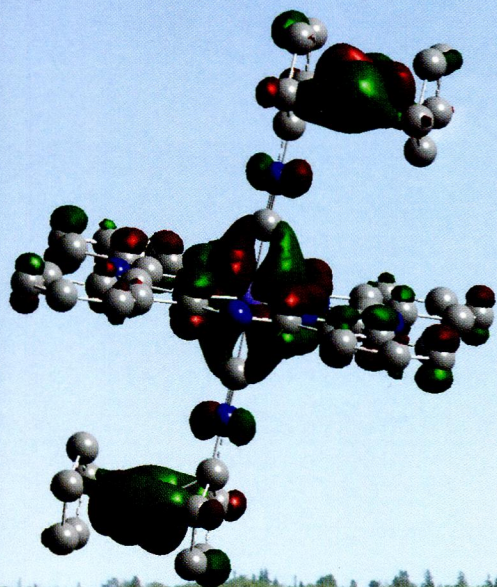


TU
1-65

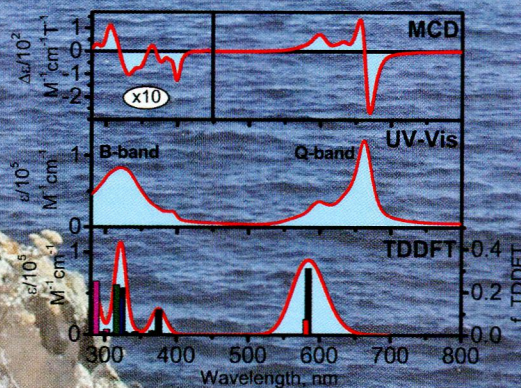
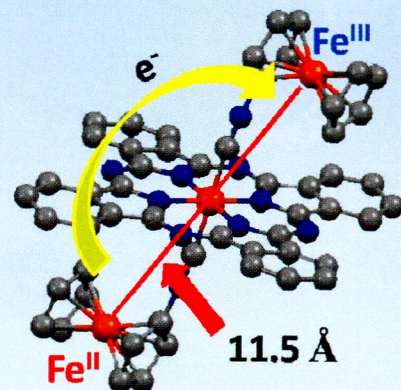
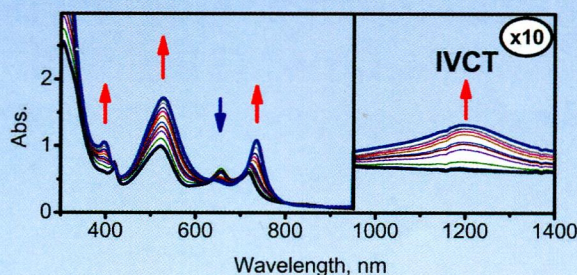
inorganic Chemistry

including bioinorganic chemistry

October 7, 2013
Volume 52, Number 19
pubs.acs.org/IC



Electron transfer in a trinuclear molecular wire



ACS Publications
MOST TRUSTED. MOST CITED. MOST READ.

www.acs.org

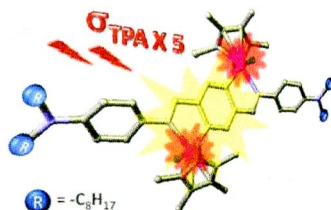

ON THE COVER: Electron-transfer properties in a trinuclear molecular wire involving isocyanoferrrocene and iron(II) phthalocyanine fragments were investigated using a variety of spectroscopic, electrochemical, and theoretical methods. See V. N. Nemykin, A. A. Purchel, A. D. Spaeth, and M. V. Barybin, p 11004. Nathan R. Erickson is kindly acknowledged for his help with the cover illustration.

Communications

10705 [dx.doi.org/10.1021/ic4012313](https://doi.org/10.1021/ic4012313)

Remarkable Effect of Iridium Cyclometalation on the Nonlinear Absorption Properties of a Quadrupolar Imine Ligand
Julien Massue, Joanna Olesiak-Banska, Erwann Jeanneau, Christophe Aronica, Katarzyna Matczyszyn, Marek Samoc, Cyrille Monnereau,* and Chantal Andraud*

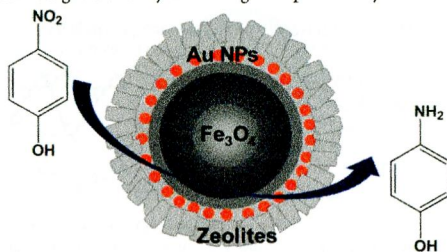
Bis-cyclometalation of a quadrupolar bis-imine ligand with an iridium(III) cation provides strong enhancement of the two- and three-photon absorption cross section of the complex compared to the ligand.

10708 [dx.doi.org/10.1021/ic401357s](https://doi.org/10.1021/ic401357s)

Fabrication and Catalytic Performance of Highly Stable Multifunctional Core–Shell Zeolite Composites

Xiaofang Wang, Yuanzheng Cui, Yang Wang, Xiaowei Song,* and Jihong Yu

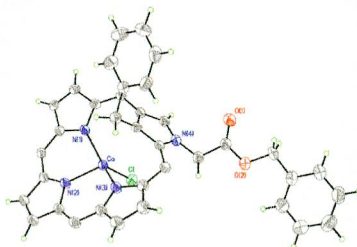
Multifunctional $Fe_3O_4@SiO_2-Au@silicalite-1$ core–shell magnetic zeolite composites were fabricated by combining a series of sol–gel process and vapor-phase transfer of silicalite-1 zeolite nanocrystal-seeded silica shells. The core–shell composites exhibit a high efficiency of magnetic separability, excellent catalytic performance, and reusability for the reduction of 4-nitrophenol. Moreover, they preserve a good stability after a high-temperature hydrothermal treatment.



Unusual Inner C-Alkylation of 2-N-Substituted N-Confused Porphyrin Cobalt Complexes in Toluene and *p*-Xylene

Yu-Cheng Wang, Jyh-Horung Chen,* Shin-Shin Wang, and Jo-Yu Tung

We report the first inner C-alkylation of solvents toluene and *p*-xylene onto the cobalt(II) complexes of N-confused porphyrin in atmospheric air under no basic conditions.

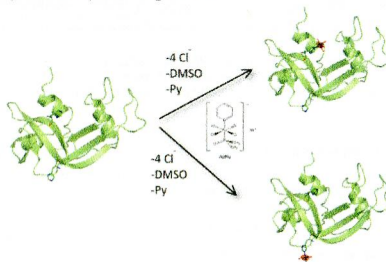


Investigating the Ruthenium Metalation of Proteins: X-ray Structure and Raman Microspectroscopy of the Complex between RNase A and AziRu

Alessandro Vergara, Irene Russo Krauss, Daniela Montesarchio, Luigi Paduano, and Antonello Merlino*

The reactivity of AziRu, a NAMI-A analogue, with RNase A was investigated by Raman microspectroscopy and X-ray crystallography. In the adduct, the Ru(III) center, upon release of its original ligands, selectively coordinates to the imidazole of His residues. AziRu inhibits the catalytic activity of the protein.

The reactivity of AziRu, a NAMI-A analogue, with RNase A was investigated by Raman microspectroscopy and X-ray crystallography. In the adduct, the Ru(III) center, upon release of its original ligands, selectively coordinates to the imidazole of His residues. AziRu inhibits the catalytic activity of the protein.



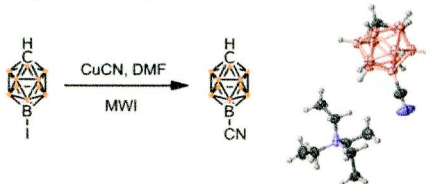
Copper-Promoted Cyanation of a Boron Cluster: Synthesis, X-ray Structure, and Reactivity of 12-CN-*closo*-CHB₁₁H₁₀⁻

Aaron J. Rosenbaum, Douglas H. Juers, and Marcus A. Juhasz*

Aaron J. Rosenbaum, Douglas H. Juers, and Marcus A. Juhasz*

Microwave-assisted cross-coupling of boron-iodinated derivatives of 1-carba-*closo*-dodecaborate(1⁻) with CuCN is shown to efficiently cyanate boron vertices of this anion. Clusters with one or two cyano groups can be prepared efficiently: 12-CNCHB₁₁H₁₀⁻ and 7,12-(CN)₂CHB₁₁H₉⁻ were synthesized in yields of 80% and 81%, respectively. The [Et₄N]⁺ salts of these anions were characterized by NMR, IR, and mass spectroscopies, and the X-ray crystal structure of [Et₄N][12-CNCHB₁₁H₁₀⁻] was determined. Hydrolysis of 12-CNCHB₁₁H₁₀⁻ gave the carboxylic acid 12-COOHCHB₁₁H₁₀⁻.

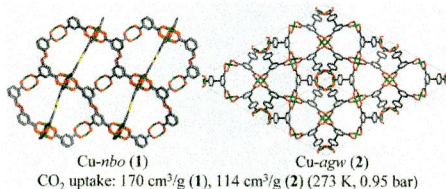
Cu-promoted cyanation of carborane anions



Design and Synthesis of Two Porous Metal–Organic Frameworks with *nbo* and *agw* Topologies Showing High CO₂ Adsorption Capacity

Zhiqiang Liang,* Jingjing Du, Libo Sun, Jin Xu, Ying Mu, Yi Li, Jihong Yu, and Ruren Xu

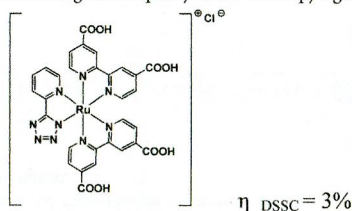
Two microporous copper-based metal–organic frameworks (MOFs) with *nbo* and *agw* topologies have been designed and synthesized based on the semirigid tetracarboxylate ligand H₄DBIP and rigid tricarboxylate ligand H₃CPEIP, respectively. These two MOFs show large surface areas up to 2314 m²/g. Compound **1** exhibits high CO₂ uptake of 170 cm³/g at 273 K and could be utilized as a reusable sorbent for CO₂ capture.



Thiocyanate-Free Ruthenium(II) Sensitizer with a Pyrid-2-yltriazolate Ligand for Dye-Sensitized Solar Cells

Claudia Dragonetti,* Alessia Colombo, Mirko Magni, Patrizia Mussini, Filippo Nisic, Dominique Roberto, Renato Ugo, Adriana Valore, Arianna Valsecchi, Paolo Salvatori, Maria Grazia Lobello, and Filippo De Angelis*

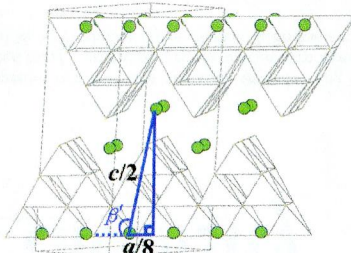
We report the synthesis of the new complex [Ru(Tetrazpy)(dcbpy)₂]Cl along with its spectroscopical, electrochemical, and theoretical characterization. The first dye-sensitized solar cell with this complex has been prepared, leading to a 3% of conversion efficiency, promising data considering the simplicity of the Tetrazpy ligand.



Quaternary Supertetrahedra-Layered Telluride CsMnInTe₃: Why Does This Type of Chalcogenide Tilt?

Hua Lin, Jin-Ni Shen, Ling Chen, and Li-Ming Wu*

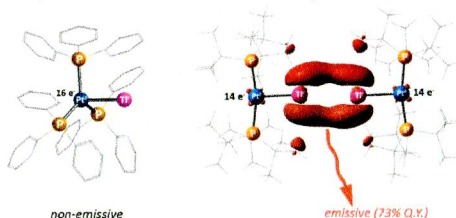
A new member of the supertetrahedra-layered chalcogenide family, CsMnInTe₃ (**1**), is discovered by a facile solid-state method using CsCl as the reactive flux. The electrostatic interactions cause tilting of the layers, and the value of the tilting angle is fixed by a structure index, $\beta' = 180^\circ - \arccos(a/4c)$. Such an index is valid for all of the members in this family known to date.



A Highly Efficient Luminescent Pt₂Tl₂ Chain with a Short Tl^I–Tl^I Interaction

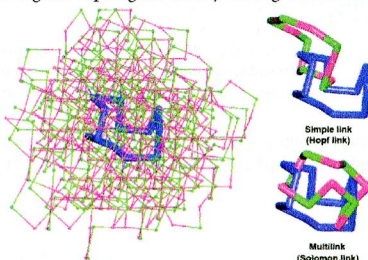
Sirous Jamali,* Mona M. Ashtiani, Zahra Jamshidi, Elena Lalinde, M. Teresa Moreno, Hamidreza Samouei, Eduardo Escudero-Adán, and Jordi Benet-Buchholz

The preparation of the first tetranuclear cluster with a rare linear metallic Pt⁰–Tl^I–Tl^I–Pt⁰ chain is described. It displays a strong red emission derived from a platinum to thallium–thallium charge-transfer excited state.

**A “Strongly” Self-Catenated Metal–Organic Framework with the Highest Topological Density among 3,4-Coordinated Nets**

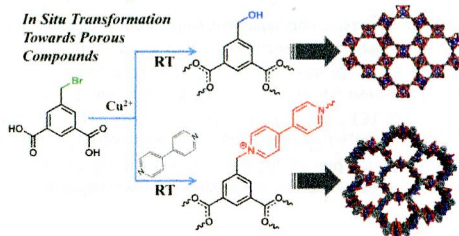
Huiqing Ma, Di Sun, Liangliang Zhang, Rongming Wang, Vladislav A. Blatov,* Jie Guo, and Daofeng Sun*

A new type of 3D “strongly” self-catenated metal–organic framework (SDU-9) has been constructed from [Cu₂(COO)₄] paddlewheel secondary building units and a tripodal carboxylate linker. Unlike the previously reported self-interpenetrated net, SDU-9 represents a rare example of a highly symmetrical coordination network and extremely tight self-catenation. To the best of our knowledge, SDU-9 has the highest topological density among all known 3,4-coordinated nets.

**In Situ Generation of Functionality in a Reactive Haloalkane-Based Ligand for the Design of New Porous Coordination Polymers**

Prakash Kanoo, Ryotaro Matsuda,* Hiroshi Sato, Liangchun Li, Hyung Joon Jeon, and Susumu Kitagawa*

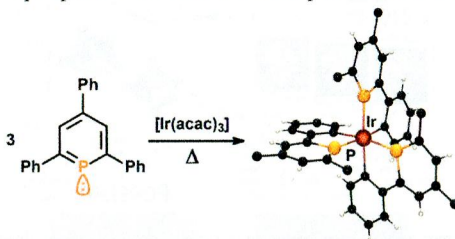
A facile synthetic approach called “in situ generation of functionality in the ligand” has been employed to isolate two new copper(II) porous coordination polymers (PCPs) via the transformation of a reactive haloalkane (CH₂Br) moiety to a neutral (CH₂OH) or a cationic functionality (–CH₂–[4,4′-bipyridine]⁺) on a isophthalate ligand at room temperature. The PCPs have free nanospace in the structure and show adsorption of CO₂ at 195 K.



C–H Activation of 2,4,6-Triphenylphosphinine: Synthesis and Characterization of the First Homoleptic Phosphinine–Iridium(III) Complex *fac*-[Ir(C[^]P)₃]

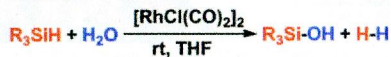
Leen E. E. Broeckx, Wyllyam Delaunay, Camille Latouche, Martin Lutz, Abdou Boucekkine,* Muriel Hissler,* and Christian Müller*

The novel homoleptic phosphinine–iridium(III) complex *fac*-[Ir(C[^]P)₃] has been prepared by C–H activation of 2,4,6-triphenylphosphinine with [Ir(acac)₃] and characterized crystallographically. This hitherto unknown species might offer new perspectives for the application of phosphinine-based coordination compounds in molecular materials science and catalysis.


Highly Efficient Generation of Hydrogen from the Hydrolysis of Silanes Catalyzed by [RhCl(CO)₂]₂

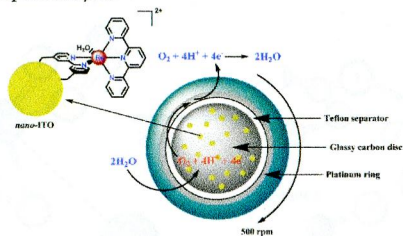
Mengmeng Yu, Huize Jing, and Xuefeng Fu*

Catalytic hydrolysis of silanes mediated by chlorodicarbonylrhodium(I) dimer [RhCl(CO)₂]₂ to produce silanols and dihydrogen efficiently under mild conditions is reported. The mixing of [RhCl(CO)₂]₂ and HSiCl₃ results in rapid formation of the key intermediate rhodium silane σ complex. Second-order kinetics and activation parameters are determined by monitoring the rate of dihydrogen evolution.


Application of the Rotating Ring-Disc-Electrode Technique to Water Oxidation by Surface-Bound Molecular Catalysts

Javier J. Concepcion, Robert A. Binstead, Leila Alibabaei, and Thomas J. Meyer*

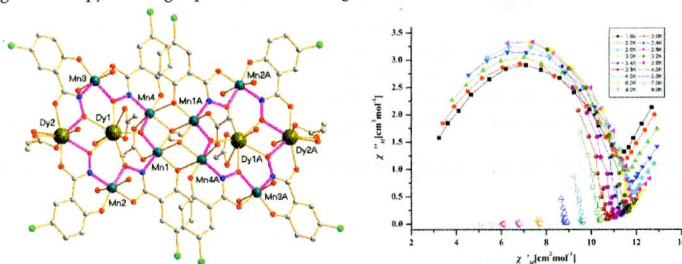
Modification of the glassy carbon disc of a rotating-ring-disc electrode with indium–tin oxide nanoparticles allows anchoring of molecular ruthenium complexes to the disc to study water oxidation catalysis. With this technique, we have been able to reliably obtain turnover frequencies, overpotentials, Faradaic conversion efficiencies, and mechanistic information from single samples of surface-bound metal complex catalysts.



Family of Mixed 3d–4f Dimeric 14-Metallacrown-5 Compounds: Syntheses, Structures, and Magnetic Properties

Fan Cao, Suna Wang, Dacheng Li, Suyuan Zeng, Meiju Niu, You Song,* and Jianmin Dou*

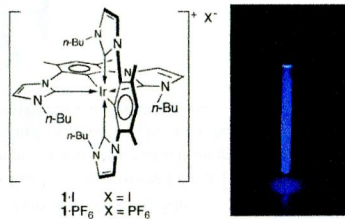
An isomorphous family of mixed 3d–4f dodecanuclear aggregates, $\{[\text{Mn}^{\text{III}}_8\text{Ln}_4(\text{Clshi})_8(\text{OAc})_6(\mu_3\text{-OCH}_3)_2(\mu_3\text{-O})_2(\text{CH}_3\text{OH})_2(\text{H}_2\text{O})_2]\cdot 4\text{CH}_3\text{OH}\cdot x\text{H}_2\text{O}\}$ ($\text{Ln} = \text{Eu}^{\text{III}}$ (1), Gd^{III} (2), Tb^{III} (3), and Dy^{III} (4); $\text{ClshiH}_3 = 5$ -chlorosalicylhydroxamic acid; $x = 5$ for 1 and 3; $x = 6$ for 2; $x = 2$ for 4), were synthesized and characterized. Each dodecanuclear aggregate contains two offset stacked 14-MC-5 units with M–N–O–M–N–O–Ln–O–N–M–O–N–M connectivity to capture one Ln^{III} ion in the core of each metallacrown. Magnetic measurements indicated that the Dy^{III} analogue with high anisotropy and large spin shows slow magnetization relaxation at a direct-current field of 2 kOe.



Efficient Near-UV Emitters Based on Cationic Bis-Pincer Iridium(III) Carbene Complexes

Noviyarn Darmawan, Cheng-Han Yang, Matteo Mauro, Matthieu Raynal, Susanne Heun, Junyou Pan, Herwig Buchholz, Pierre Braunstein, and Luisa De Cola*

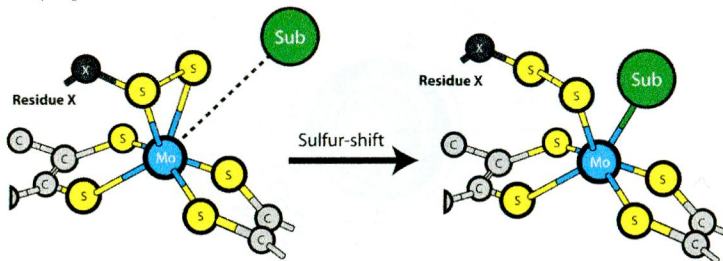
Cationic near-UV emitters based on bis-pincer Ir(III) carbene complexes are reported. In the solid state, the complexes show an interesting photophysical behavior that depends on the counterion.



The Sulfur Shift: An Activation Mechanism for Periplasmic Nitrate Reductase and Formate Dehydrogenase

Nuno M. F. S. A. Cerqueira,* Pedro A. Fernandes, Pablo J. Gonzalez, José J. G. Moura, and Maria J. Ramos

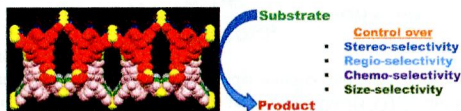
The sulfur-shift mechanism is characterized by the displacement of the coordinating cysteine (in Nap or SeCys in Fdh) side chain to a second shell of the Mo-coordination sphere. This rearrangement enables a free coordination position for substrate binding to Mo ion and provides an efficient mechanism to maintaining a constant coordination number throughout the entire catalytic pathway. This type of mechanism is very similar to the carboxylate shift observed in other enzymes, and it has been recently detected by experimental means.



Three-Dimensional $\{Co^{3+}-Zn^{2+}\}$ and $\{Co^{3+}-Cd^{2+}\}$ Networks Originated from Carboxylate-rich Building Blocks: Syntheses, Structures, and Heterogeneous Catalysis

Girijesh Kumar and Rajeev Gupta*

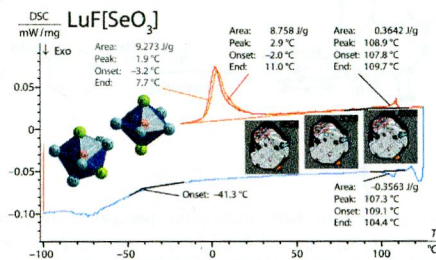
Co^{3+} complexes appended with *para*- or *meta*-arylcarboxylates are utilized as the molecular building blocks for preparing extended $\{Co^{3+}-Zn^{2+}\}$ and $\{Co^{3+}-Cd^{2+}\}$ networks. The structurally characterized networks function as the heterogeneous and reusable catalysts for the regio-, stereo-, and chemoselective ring-opening reactions of epoxides and size-selective cyanation reactions of aldehydes.



$LuF[SeO_3]$: The Structural Chameleon of Lanthanoid Fluoride Oxoselenates(IV)

Christian Lipp, Robert E. Dinnebier, and Thomas Schleid*

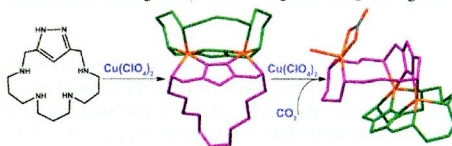
$LuF[SeO_3]$ is a compound that can easily be obtained by a solid-state reaction of Lu_2O_3 , LuF_3 , and SeO_2 with CsBr as the fluxing agent. The outstanding property of $LuF[SeO_3]$ is the appearance of two phase transitions within a range of less than 200 K.



Intermolecular Binding Modes in a Novel [1 + 1] Condensation 1*H*-Pyrazole Azamacrocyclic: A Solution and Solid State Study with Evidence for CO₂ Fixation

Raquel Belda, Javier Pitarch-Jarque, Conxa Soriano, José M. Llinares, Salvador Blasco, Jesús Ferrando-Soria, and Enrique García-España*

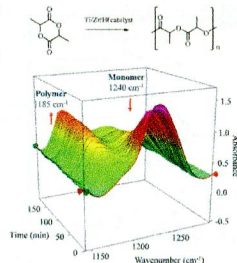
A novel [1+1] pyrazole cyclophane forms dimeric dinuclear copper(II) complexes leaving free donor atoms which can bind a further copper(II) giving rise to a molecular arrangement able to capture CO₂ with great affinity.



Synthesis and Structural Characterization of Group 4 Metal Alkoxide Complexes of *N,N,N',N'*-Tetrakis(2-hydroxyethyl)ethylenediamine and Their Use As Initiators in the Ring-Opening Polymerization (ROP) of *rac*-Lactide under Industrially Relevant Conditions

Christopher J. Chuck, Matthew G. Davidson,* Gerrit Gobius du Sart, Petya K. Ivanova-Mitseva, Gabriele I. Kociok-Köhn, and Lois B. Manton

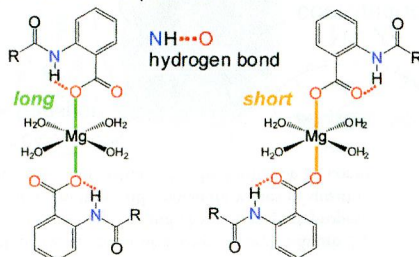
A series of *N,N,N',N'*-tetrakis(2-hydroxyethyl)ethylenediamine (TOEDH₄) ligand precursors and their group 4 metal complexes are reported. Initial catalytic data are presented for the polymerization of *rac*-lactide (*rac*-LA) under melt conditions. The ability to systematically vary the number of TOED ligands within the complex was investigated. All of the catalysts screened showed reasonable activity, although the most promising catalyst, Ti₄(TOED)(*O*Pr)₁₂, was demonstrated to convert over 95% of the *rac*-LA within 160 minutes under industrially relevant conditions.



Contribution of Intramolecular NH...O Hydrogen Bonds to Magnesium–Carboxylate Bonds

Taka-aki Okamura* and Junko Nakagawa

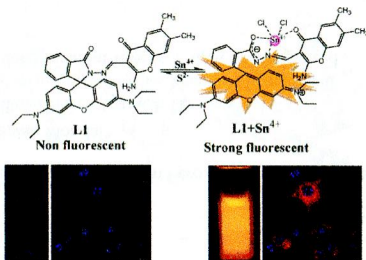
Magnesium carboxylate complexes containing intramolecular NH...O hydrogen bonds were synthesized. Their molecular structures were determined by X-ray analysis. A direct NH...O hydrogen bond to the coordinated oxygen atom elongated the Mg–O bond, while a hydrogen bond to the carbonyl group shortened the Mg–O bond. Double NH...O hydrogen bonds significantly lowered the basicity of the carboxylate anion and prevented coordination to the Mg ion in a *trans* configuration; however, a *cis*-dicarboxylate complex was successfully obtained.



Highly Sensitive and Selective Rhodamine-Based “Off–On” Reversible Chemosensor for Tin (Sn^{4+}) and Imaging in Living Cells

Ajit Kumar Mahapatra,* Saikat Kumar Manna, Debasish Mandal, and Chitragada Das Mukhopadhyay

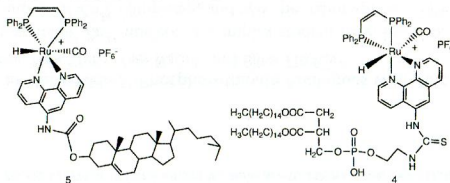
A structurally characterized new oxo-chromene functionalized rhodamine derivative **L1** exhibits high selectivity toward Sn^{4+} by forming a 1:1 complex, among other biologically important metal ions, as studied by fluorescence, absorption, and HRMS spectroscopy. The sensor shows extremely high fluorescence enhancement upon complexation with Sn^{4+} , and it can be used as a “naked-eye” sensor. Further, confocal microscopic studies confirmed that the receptor shows *in vitro* detection of Sn^{4+} ions in RAW cells.



Photophysical Studies of Bioconjugated Ruthenium Metal–Ligand Complexes Incorporated in Phospholipid Membrane Bilayers

Ayesha Sharmin, Luca Salassa, Edward Rosenberg,* J. B. Alexander Ross,* Geoffrey Abbott, Labe Black, Michelle Terwilliger, and Robert Brooks

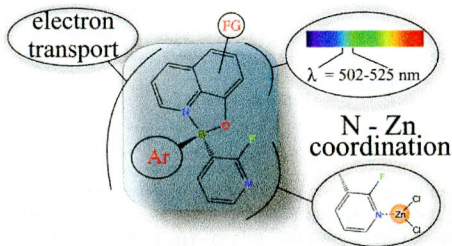
The luminescent, monodimine ruthenium complexes $[(\text{H})\text{Ru}(\text{CO})(\text{PPh}_3)_2(4,4'\text{-dicarboxy-2,2'\text{-bipyridyl})][\text{PF}_6^-]$ (**1**) and $[(\text{H})\text{Ru}(\text{CO})(\text{bis}(\text{diphenylphosphino})\text{ethylene})(5\text{-amino-1,10-phenanthroline})][\text{PF}_6^-]$ (**2**) were conjugated with 1,2-dihexadecanoyl-*sn*-glycero-3-phosphoethanolamine and with cholesterol in the case of complex **2**. The photophysical properties of the complexes were studied in solution in lipid bilayer vesicles and the results interpreted in terms of the factors affecting the metal-to-ligand charge transfer bands in these environments.



Heteroleptic (2-Fluoro-3-pyridyl)arylboronic 8-Oxyquinolates for the Potential Application in Organic Light-Emitting Devices

Grzegorz Wesela-Bauman,* Paulina Ciechwierz, Krzysztof Durka, Sergiusz Luliński,* Janusz Serwatowski, and Krzysztof Woźniak

The synthesis and physicochemical characterization of a series of aryl(2-fluoro-3-pyridyl)boronic 8-oxyquinolates are reported. The discussion of optical, electrochemical, and charge-transport properties is supported by computational studies. The obtained complexes are green-type emitters with moderate values of quantum yields. They can act as fluorescent functionalized pyridyl ligands, which was demonstrated by the formation of complexes with ZnCl_2 .



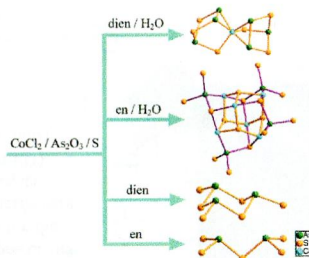
10860 **S**

dx.doi.org/10.1021/ic4007982

Clusters $[\text{Co}(\text{As}_3\text{S}_3)_2]^{2-}$, $[\text{Ni}(\text{As}_3\text{S}_3)_2]^{2-}$, and $[\{\text{Co}(\text{en})\}_6(\mu_3\text{-S})_4(\text{AsS}_3)_4]^{2-}$ with Co–As or Ni–As Bonds: Solvothermal Syntheses and Characterizations of Thioarsenates Containing Transition-Metal Complexes

Chunying Tang, Fang Wang, Wenqing Jiang, Yong Zhang, and Dingxian Jia*

The first $[\text{Co}(\text{As}_3\text{S}_3)_2]^{2-}$, $[\text{Ni}(\text{As}_3\text{S}_3)_2]^{2-}$, and $[\{\text{Co}(\text{en})\}_6(\mu_3\text{-S})_4(\text{AsS}_3)_4]^{2-}$ clusters containing thioarsenate ligands with both As- and S-donor atoms were prepared by the reactions of As_2O_3 and S with $\text{CoCl}_2 \cdot 6\text{H}_2\text{O}$ or $\text{NiCl}_2 \cdot 6\text{H}_2\text{O}$ in aqueous solutions of dien and en under solvothermal conditions. The same reactions in pure dien and en solvents afforded compounds with discrete thioarsenate anions $[\text{As}_3\text{S}_6]^{3-}$ and $[\text{As}_2\text{S}_4]^{4-}$, respectively.



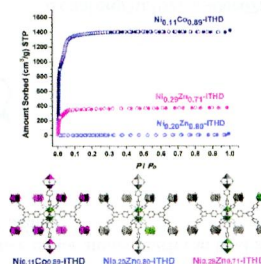
10869

dx.doi.org/10.1021/ic400844v

Hybrid Bimetallic Metal–Organic Frameworks: Modulation of the Framework Stability and Ultralarge CO_2 Uptake Capacity

Xiaokai Song, Minhak Oh, and Myoung Soo Lah*

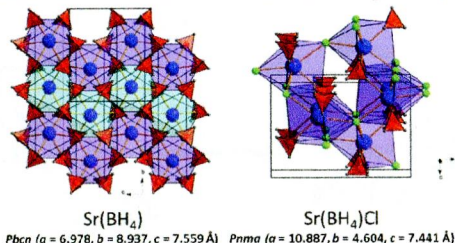
The ultraporeous hybrid bimetallic $\text{Ni}_{0.11}\text{Co}_{0.89}$ -ITHD with only ≈ 0.1 mol fraction Ni(II) ion doping showed enhanced framework stability, comparable to that of pure Ni-ITHD. The CO_2 uptake capacity of the hybrid bimetallic $\text{Ni}_{0.11}\text{Co}_{0.89}$ -ITHD, which was activated via the conventional vacuum drying process, at 1 bar and 195 K is larger than those of any other reported MOFs under similar conditions, and the excess CO_2 uptake capacity at 40 bar and 295 K is comparable to those of other MOFs that were activated via the supercritical carbon dioxide drying process, with similar pore volumes.



Novel Alkali Earth Borohydride $\text{Sr}(\text{BH}_4)_2$ and Borohydride-Chloride $\text{Sr}(\text{BH}_4)\text{Cl}$

D. B. Ravnsbæk,* E. A. Nickels, R. Černý, C. H. Olesen, W. I. F. David, P. P. Edwards, Y. Filinchuk, and T. R. Jensen

The synthesis, structure, and thermal decomposition pathway of two novel alkali earth borohydrides, $\text{Sr}(\text{BH}_4)_2$ and $\text{Sr}(\text{BH}_4)\text{Cl}$, are presented. $\text{Sr}(\text{BH}_4)_2$ consists of a framework of slightly distorted $[\text{Sr}(\text{BH}_4)_6]$ octahedra stacked in half-occupied brucite-like layers. The $\text{Sr}(\text{BH}_4)\text{Cl}$ framework is built from (011) layers of edge-sharing $[\text{Sr}(\text{BH}_4)_2\text{Cl}_4]$ monocapped trigonal prisms. $\text{Sr}(\text{BH}_4)\text{Cl}$ dissociates to $\text{Sr}(\text{BH}_4)_2$ and SrCl_2 at $T \approx 170^\circ\text{C}$, while $\text{Sr}(\text{BH}_4)_2$ decomposes at $T \approx 350^\circ\text{C}$ with formation of multiple decomposition intermediates and SrB_6 as the final decomposition product.



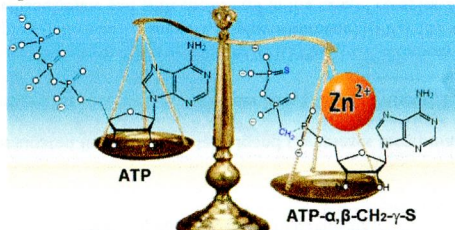
10886 5

dx.doi.org/10.1021/ic400878k

Characterization of Complexes of Nucleoside-5'-Phosphorothioate Analogues with Zinc Ions

Alon Haim Sayer, Yehudit Itzhakov, Noa Stern, Yael Nadel, and Bilha Fischer*

$\text{ATP-}\alpha,\beta\text{-CH}_2\text{-}\gamma\text{-S}$ formed the most stable Zn^{2+} -nucleotide complex studied here, $\log K$ 6.50, being ~ 0.8 and ~ 1.1 log units more stable than $\text{ATP-}\gamma\text{-S-Zn}^{2+}$ and ATP-Zn^{2+} complexes, and was the major species, 84%, under physiological pH. $^1\text{H-}$ and ^{31}P NMR monitored Zn^{2+} titration showed that Zn^{2+} coordinates with the purine nucleotide N7-nitrogen atom, the terminal phosphate, and the adjacent phosphate.



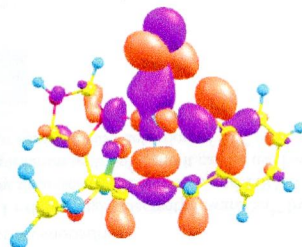
10897 5

dx.doi.org/10.1021/ic400890f

Reaction of a Copper(II)–Nitrosyl Complex with Hydrogen Peroxide: Phenol Ring Nitration through a Putative Peroxynitrite Intermediate

Apurba Kalita, Ramesh C. Deka, and Biplab Mondal*

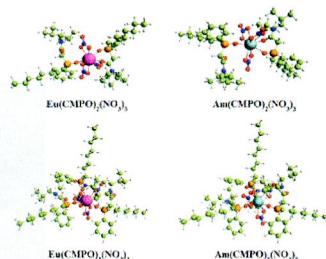
Copper(II) complex, **1**, with the histidine-derived ligand **L** (**L** = methyl 2-(2-hydroxybenzylamino)-3-(1H-imidazol-5-yl)propanoate) has been synthesized and characterized. Single-crystal structure determination reveals a diphenolato-bridged dicopper(II) core in **1**.



Complexation Behavior of Eu(III) and Am(III) with CMPO and Ph₂CMPO Ligands: Insights from Density Functional Theory

Cong-Zhi Wang, Wei-Qun Shi,* Jian-Hui Lan, Yu-Liang Zhao, Yue-Zhou Wei, and Zhi-Fang Chai*

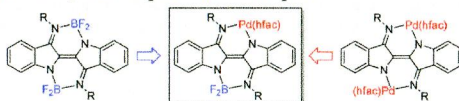
The Eu(III) and Am(III) extraction complexes with CMPO (*n*-octyl(phenyl)-*N,N*-diisobutyl-methylcarbamoyl phosphine oxide) in nitric acid solutions have been studied using the density functional theory (DFT) method.



Synthesis and Characterization of Heterobimetallic (Pd/B) Nindigo Complexes and Comparisons to Their Homobimetallic (Pd₂, B₂) Analogues

Graeme Nawn, Robert McDonald, and Robin G. Hicks*

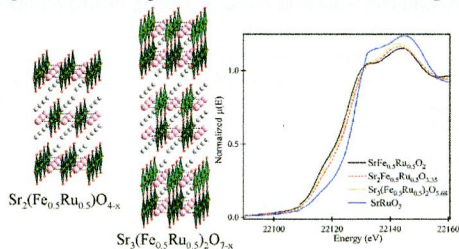
The first mixed-metal (Pd/B) complexes of the Nindigo bridging ligand are reported. Comparisons of the electronic structure of the new complexes with those of their homobimetallic (Pd₂, B₂) analogues are undertaken using a combination of spectroscopic, structural, electrochemical, and computational techniques.



Topochemical Reduction of the Ruddlesden–Popper Phases Sr₂Fe_{0.5}Ru_{0.5}O₄ and Sr₃(Fe_{0.5}Ru_{0.5})₂O₇

Fabio Denis Romero, Diego Gianolio, Giannantonio Cibin, Paul A. Bingham, Jeanne-Clotilde d'Hollander, Susan D. Forder, and Michael A. Hayward*

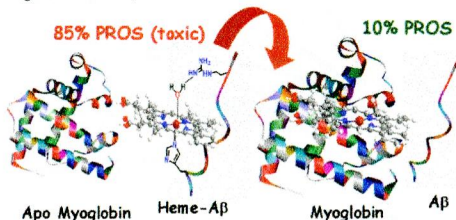
Reaction of Ruddlesden–Popper phases Sr₂Fe_{0.5}Ru_{0.5}O₄ and Sr₃(Fe_{0.5}Ru_{0.5})₂O₇ with CaH₂ results in the topochemical deintercalation of oxide ions from these materials and the formation of samples with average compositions of Sr₂Fe_{0.3}Ru_{0.5}O_{3.35} and Sr₃(Fe_{0.5}Ru_{0.5})₂O_{5.68}, respectively. X-ray absorption data reveal the reduced samples contain an Fe³⁺ and Ru^{2+/3+} oxidation state combination, which is unexpected considering the Fe³⁺/Fe²⁺ and Ru³⁺/Ru²⁺ redox potentials.



Apomyoglobin Sequesters Heme from Heme Bound A β Peptides

Debajyoti Pramanik, Soumya Mukherjee, and Somdatta Ghosh Dey*

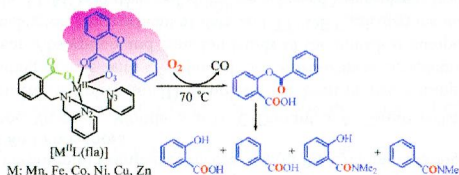
Heme bound A β peptide has been invoked to be associated with AD. Oxidized heme-A β complexes exhibit peroxidase activity, and reduced heme-A β complexes are prone to PROS generation. Apo Myoglobin (apoMb) can sequester heme from heme-A β in both the oxidized and the reduced forms. The rate of heme transfer follows biphasic kinetics. These results might exhibit a protective role played by apoMb against heme-A β .



Flavonolate Complexes of M^{II} (M = Mn, Fe, Co, Ni, Cu, and Zn). Structural and Functional Models for the ES (Enzyme–Substrate) Complex of Quercetin 2,3-Dioxygenase

Ying-Ji Sun,* Qian-Qian Huang, Tetsuro Tano, and Shinobu Itoh

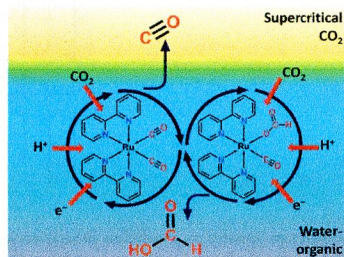
A series of flavonolate complexes [M^{II}L(flal)] (M = Mn, Fe, Co, Ni, Cu, and Zn) are reported as structural and functional ES (enzyme–substrate) models of various M^{II}-containing quercetin 2,3-dioxygenase (2,3-QD), which exhibit notably different high enzyme-like dioxygenation reactivity (oxidative ring-opening of substrate flavonolate) due to the existing carboxylate group in the ligand, providing important insights into the metal ion effects on the enzymatic reactivity of metal-substituted 2,3-QD.



Photoreduction of CO₂ Using [Ru(bpy)₂(CO)]²⁺ Catalysts in Biphasic Solution/Supercritical CO₂ Systems

Patrick Voyame, Kathryn E. Toghil, Manuel A. Méndez, and Hubert H. Girault*

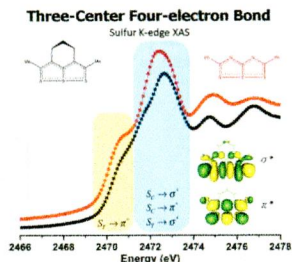
The photosensitized reduction of carbon dioxide by the molecular catalyst [Ru(bpy)₂(CO)L] is studied in a biphasic liquid-condensed gas system. Increasing pressure is shown to enhance the initial production rate and turnover number of the catalyst before deactivation of the system, especially for formation of carbon monoxide.



Bond Characterization of a Unique Thiathiophthene Derivative: Combined Charge Density Study and X-ray Absorption Spectroscopy

Yu-Chun Chuang, Ya-Wen Li, I-Jui Hsu, Gene-Hsiang Lee, and Yu Wang*

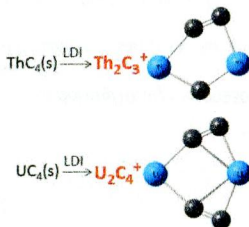
The unique 10π electron and a three-center four-electron S–S–S σ bond of the TTP fragment is characterized based on a charge density study and sulfur K-edge X-ray absorption.



Thorium and Uranium Carbide Cluster Cations in the Gas Phase: Similarities and Differences between Thorium and Uranium

Cláudia C. L. Pereira, Rémi Maurice, Ana F. Lucena, Shuxian Hu, António P. Gonçalves, Joaquim Marçalo,* John K. Gibson, Lester Andrews, and Laura Gagliardi*

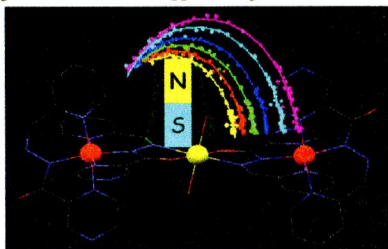
Laser ionization of solid thorium and uranium carbide targets resulted in molecular actinide carbide clusters. Intriguing high abundances for both ThC_{13}^+ and UC_{13}^+ and for $\text{Th}_{13}\text{C}_n^+$ were observed. A disparity between An = Th and U in the relative abundances of the bimetallic ions An_2C_3^+ and An_2C_4^+ was apparent and elucidated by computations based on density functional theory.



Tuning Transverse Anisotropy in $\text{Co}^{\text{III}}\text{--Co}^{\text{II}}\text{--Co}^{\text{III}}$ Mixed-Valence Complex toward Slow Magnetic Relaxation

Dayu Wu,* Xingxing Zhang, Ping Huang, Wei Huang, Mingyue Ruan, and Z. W. Ouyang*

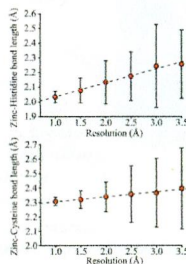
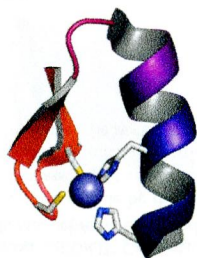
Through tuning of the small differences in transverse anisotropy, a mononuclear $\text{Co}(\text{II})$ complex with a hard axis was revealed to exhibit slow relaxation of the magnetization under an applied magnetic field.



Zinc Coordination Spheres in Protein Structures

Mikko Laitaoja, Jarkko Valjakka, and Janne Jänis*

A statistical analysis in terms of zinc coordinating amino acids, metal-to-ligand bond lengths, coordination number, and structural classification was performed, revealing coordination spheres from classical tetrahedral cysteine/histidine binding sites to more complex binuclear sites with carboxylated lysine residues. According to the results, coordination spheres of hundreds of crystal structures in the PDB could be misinterpreted due to symmetry-related molecules or missing electron densities for ligands.



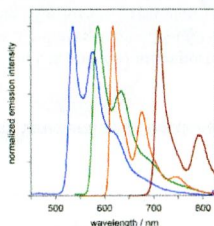
10992 5

dx.doi.org/10.1021/ic401131x

Highly Luminescent Dinuclear Platinum(II) Complexes Incorporating Bis-Cyclometalating Pyrazine-Based Ligands: A Versatile Approach to Efficient Red Phosphors

Stacey Culham, Pierre-Henri Lanoë, Victoria L. Whittle, Marcus C. Durrant, J. A. Gareth Williams,* and Valery N. Kozhevnikov*

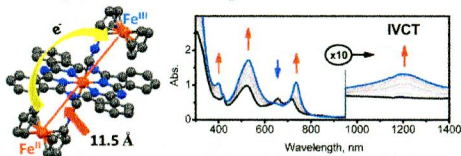
A family of new dinuclear cyclometalated platinum(II) complexes has been prepared using diphenylpyrazine-based compounds as bis- N^C -coordinating ligands, with O^O -bound dipivaloylmethane completing the coordination sphere. All of the complexes are phosphorescent. Absorption and emission bands of the dinuclear compounds are strongly red shifted relative to their mononuclear analogues. Electrochemical data and TD-DFT calculations indicate that this effect arises primarily from stabilization of the LUMO. Further red shifts are achieved using planar bridging ligands featuring more extended conjugation.



Probing the Electronic Properties of a Trinuclear Molecular Wire Involving Isocyanoferrrocene and Iron(II) Phthalocyanine Motifs

Victor N. Nemykin,* Anatolii A. Purchel, Andrew D. Spaeth, and Mikhail V. Barybin*

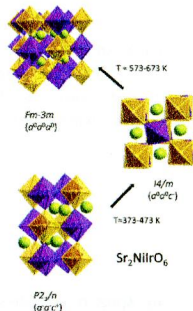
A new trinuclear iron(II) organometallic complex consisting of two isocyanoferrrocene ligands axially coordinated to iron(II) phthalocyanine has been isolated and characterized using UV-vis, magnetic circular dichroism, NMR spectroscopies, and X-ray crystallography. The redox behavior of this molecular wire was investigated by means of electrochemical, spectroelectrochemical, and chemical oxidation approaches and compared to that of the bis(*tert*-butylisocyanine)iron(II) phthalocyanine reference compound. The spectroscopic and redox properties of the title and reference complexes were correlated with density functional theory (DFT) and time-dependent DFT data.



Crystal Structure, Phase Transitions, and Magnetic Properties of Iridium Perovskites Sr_2MIrO_6 ($M = \text{Ni}, \text{Zn}$)

P. Kayser,* M. J. Martínez-Lope, J. A. Alonso, M. Retuerto, M. Croft, A. Ignatov, and M. T. Fernández-Díaz

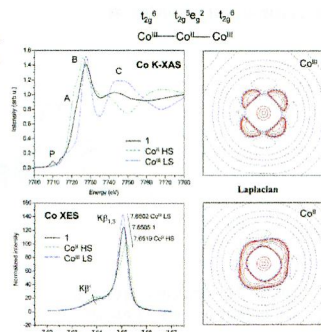
Title double perovskites present an ordered arrangement of the B-site cations at room temperature, and that its structure at RT can be described with the $P2_1/n$ space group. A XANES study gives a complementary insight of the oxidation states of 3d and Ir ions. The study of the temperature dependence of the crystal structure shows the presence of two phase transitions for $\text{Sr}_2\text{NiIrO}_6$ compound in the 373–673 K interval.



Chemical Bond Characterization of a Mixed-Valence Tri-Cobalt Complex, $\text{Co}_2(\mu\text{-admrz})_2(\mu\text{-OH})_2(\text{CN})_6\cdot 2\text{H}_2\text{O}$

Lai-Chin Wu, Tsu-Chien Weng, I-Jui Hsu,* Yi-Hung Liu, Gene-Hsiang Lee, Jyh-Fu, Lee, and Yu Wang*

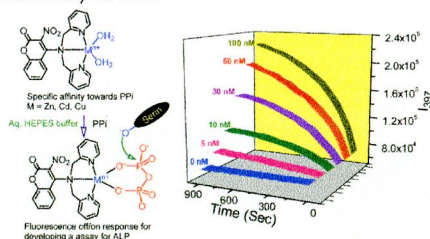
The linear tri-cobalt complex is firmly characterized as a mixed valence complex with two terminal Co^{III} at a low spin and a central Co^{II} at a high spin state through electron density distribution (XRD) and Co K-edge X-ray absorption and emission (XAS and XES).



Role of Metal Ion in Specific Recognition of Pyrophosphate Ion under Physiological Conditions and Hydrolysis of the Phosphoester Linkage by Alkaline Phosphatase

Priyadip Das, Nellore Bhanu Chandar, Shishir Chourey, Hridesh Agarwalla, Bishwajit Ganguly,* and Amitava Das*

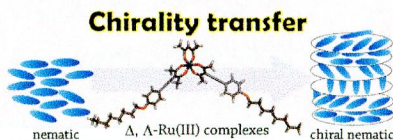
Metal complexes as fluorescence-based assay for ALP.



Tris(β -diketonato) Ru(III) Complexes as Chiral Dopants for Nematic Liquid Crystals: the Effect of the Molecular Structure on the Helical Twisting Power

Jun Yoshida,* Go Watanabe, Kaori Kakizawa, Yasuhiro Kawabata, and Hidetaka Yuge

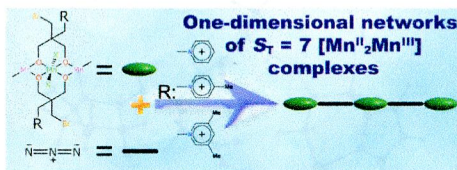
A series of Δ -, Λ -Ru(III) complexes have been synthesized to investigate their helical twisting powers for nematic liquid crystals.



Synthesis of an $S_T = 7$ $[Mn_3]$ Mixed-Valence Complex Based on 1,3-Propanediol Ligand Derivatives and Its One-Dimensional Assemblies

Jian Huang, Gang Wu,* Jiaquan Bai, Yuan Jiang, Guanghua Li, Shilun Qiu,* and Rodolphe Cl  rac*

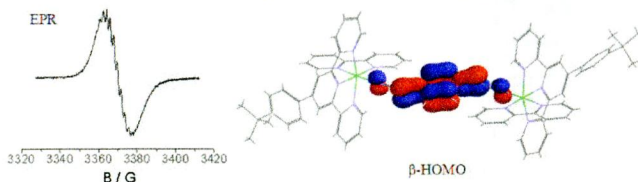
A discrete high-spin ($S_T = 7$) $[Mn^{II}_2Mn^{III}]$ complex and its one-dimensional assemblies were successfully synthesized using pyridinium-functionalized 1,3-propanediol derivatives and azido anions as chelating and bridging ligands, respectively. The syntheses, characterization, crystal structures, and magnetic properties of these four new $[Mn_3]$ -based magnetic materials are reported.



Non-Innocence of 1,4-Dicyanamidobenzene Bridging Ligands in Dinuclear Ruthenium Complexes.

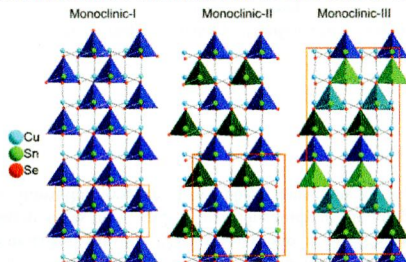
Mohammad M. R. Choudhuri, Wolfgang Kaim, Biprajit Sarkar, and Robert J. Crutchley*

EPR, visible/NIR, and IR spectroelectrochemical studies of $[\{Ru(ttpy)(bpy)\}_2(\mu-L)]^{3+}$ ions, where L is a substituted 1,4-dicyanamidobenzene, determined that the ground state description is mainly $[Ru(II), L^{\cdot-}, Ru(II)]^{3+}$ with the degree of Ru(III) character dependent on the nature of the dicyanamidebenzene bridging ligand.

**New Monoclinic Phase at the Composition Cu_2SnSe_3 and Its Thermoelectric Properties**

Jing Fan, Wilder Carrillo-Cabrera, Lev Akselrud, Iryna Antonyshyn, Lidong Chen, and Yuri Grin*

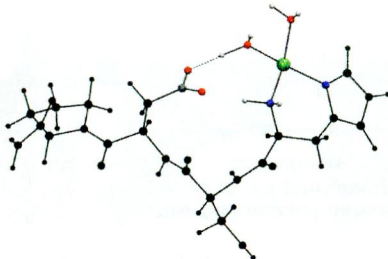
The crystal structure of a new monoclinic phase (monoclinic-II) of $m2-Cu_2SnSe_3$ is solved through electron diffraction tomography analysis, and then refined using the high resolution synchrotron X-ray powder diffraction data. A phase transformation to cubic crystal structure was observed. According to quantum chemical calculations, $m2-Cu_2SnSe_3$ is a narrow-gap semiconductor, confirmed by its thermoelectric properties. Electron localizability approach was applied to study the chemical bonding. A comparison with monoclinic-I and monoclinic-III modifications was given.



Zinc(II) Interactions with Brain-Derived Neurotrophic Factor N-Terminal Peptide Fragments: Inorganic Features and Biological Perspectives

Alessio Travaglia, Diego La Mendola,* Antonio Magri, Adriana Pietropaolo, Vincenzo G. Nicoletti, Giuseppe Grasso, Gaetano Malgieri, Roberto Fattorusso, Carla Isernia, and Enrico Rizzarelli

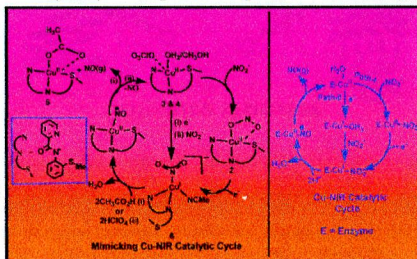
The predominant complex species formed by a BDNF terminal domain peptide fragment with Zn^{2+} is $[ZnL]^{2+}$, in which the metal ion is bound to one amino, one imidazole, and two water molecules (NH_2 , N_{Im} , and $2O_{water}$) in a tetrahedral environment. DFT-based geometry optimization of zinc coordination showed a hydrogen bond between the carboxylate and a water molecule bound to the metal ion.



Copper Complexes Relevant to the Catalytic Cycle of Copper Nitrite Reductase: Electrochemical Detection of NO(g) Evolution and Flipping of NO_2 Binding Mode upon $Cu^{II} \rightarrow Cu^I$ Reduction

Ram Chandra Maji, Suman Kumar Barman, Suprakash Roy, Sudip K. Chatterjee, Faye L. Bowles, Marilyn M. Olmstead, and Apurba K. Patra*

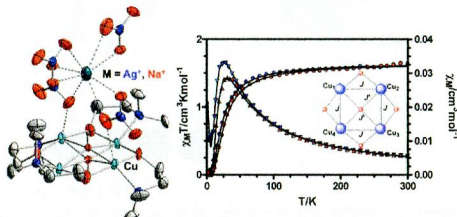
$Cu^{II/I}$ complexes of a tridentate monocarboxamide ligand have been synthesized and characterized. Present set of complexes mimic many of the steps of CuNIR catalytic cycle for proton coupled reduction of copper-coordinated $NO_2^- \rightarrow NO(g)$.



Structural Diversity due to Amino Alcohol Ligands Leading to Rare μ_4 -Hydroxo-Bridged Tetranuclear and "Bicapped Cubane" Cores in Copper(II) Complexes: A Theoretical and Experimental Magnetostructural Study

Petri Seppälä, Enrique Colacio,* Antonio J. Mota, and Reijo Sillanpää*

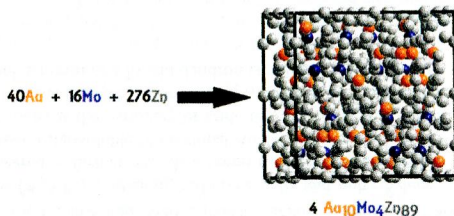
The syntheses, crystal structures and magnetic properties of three μ_4 -hydroxo- and alkoxo-bridged tetranuclear copper(II) complexes 1-3 and hexanuclear alkoxo-bridged "bicapped cubane" copper(II) complex 8 are reported. The tetranuclear complexes represent rare copper compounds with a $\text{Cu}_4(\mu_4\text{-OH})$ core. Also two new copper(II) amino alcohol complexes, one heterometallic Cu(II)/Ag(I) amino alcohol complex, and one silver(I) oxazino-oxazine complex (4–7) were obtained and their crystal structures are reported.



$\text{Au}_{10}\text{Mo}_4\text{Zn}_{89}$: A Fully Ordered Complex Intermetallic Compound Analyzed by TOPOS

Partha P. Jana,* Arina A. Pankova, and Sven Lidin

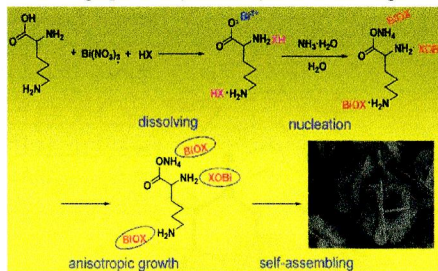
The structure of $\text{Au}_{10}\text{Mo}_4\text{Zn}_{89}$ is complex yet ordered. The structure of the ordered $\text{Au}_{10}\text{Mo}_4\text{Zn}_{89}$ compound has been described by using the algorithm of automatic geometric and topological analysis that is implemented in TOPOS as the "Nanoclustering" procedure. This method is useful for understanding complex crystal structure. The electronic structure calculation on the refined ordered structure of $\text{Au}_{10}\text{Mo}_4\text{Zn}_{89}$ reveals a pronounced pseudogap on density of state around the Fermi level for the compound, which is consistent with the γ -brass-type phase or related phases.



Room-Temperature Synthesis of Flower-Like BiOX (X=Cl, Br, I) Hierarchical Structures and Their Visible-Light Photocatalytic Activity

Lang Chen, Rui Huang, Miao Xiong, Qing Yuan, Jie He, Jing Jia, Meng-Yuan Yao, Sheng-Lian Luo, Chak-Tong Au, and Shuang-Feng Yin*

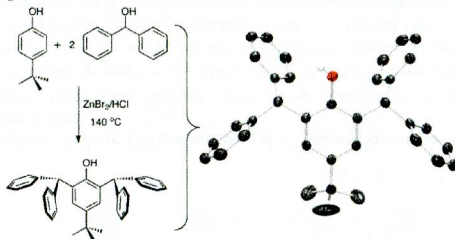
A simple method for facile synthesis of three-dimensional (3D) bismuth oxyhalide (BiOX, X=Cl, Br, I) hierarchical structures at room temperature has been developed. All of the processes are conducted under environmentally-friendly conditions using water as solvent and L-lysine as surfactant (biomolecular). The BiOX (X=Cl, Br, I) hierarchical architectures are composed of single-crystalline nanoplates. An amino-and-carboxyl structure-directing mechanism for the formation of the hierarchical structures is proposed. All samples show high photocatalytic activity under visible light.



3d Early Transition Metal Complexes Supported by a New Sterically Demanding Aryloxy Ligand

Keith Searles, Ba L. Tran, Maren Pink, Chun-Hsing Chen, and Daniel J. Mindiola*

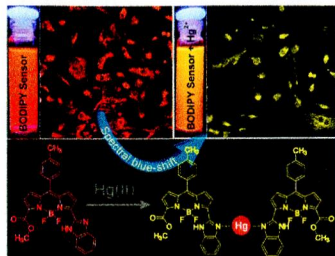
A highly arylated and sterically demanding alkoxide ligand has been prepared, and its coordination chemistry with some early 3d transition metals has been explored.



Sensing Hg(II) *In Vitro* and *In Vivo* Using a Benzimidazole Substituted BODIPY

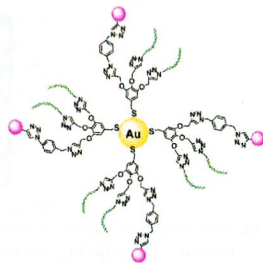
Sheri Madhu, Dharmendar Kumar Sharma, Santanu Kumar Basu, Sameer Jadhav, Arindam Chowdhury,* and Mangalampalli Ravikanth*

A multisignaling Hg(II) sensor based on a benzimidazole substituted BODIPY framework was designed, the optical and fluorogenic measurements performed in solution revealed that the sensor can detect mercury ions at submicromolar concentrations, and with high specificity over other heavy and transition-metal ions under physiological conditions. The utility of this BODIPY sensor to detect Hg(II) *in vivo* was demonstrated by spectrally resolved fluorescence imaging of sensors within human breast adenocarcinoma cells.

**"Click" Star-Shaped and Dendritic PEGylated Gold Nanoparticle-Carborane Assemblies**

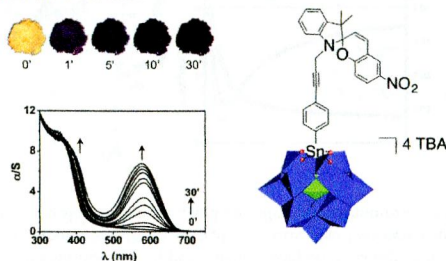
Na Li, Pengxiang Zhao, Lionel Salmon, Jaime Ruiz, Mark Zabawa, Narayan S. Hosmane,* and Didier Astruc*

Biocompatible gold nanoparticles (AuNPs) containing carborane units and polyethylene glycol (PEG) tethers were engineered to further provide a boron neutron capture therapy (BNCT) platform. Therefore these water-soluble bifunctional AuNPs were synthesized either through two-step click reactions at the periphery of azido-terminated AuNPs in the presence of the efficient catalyst $[Cu^I tren(CH_2Ph)_6][Br]$ or simply by direct stabilization of AuNPs using a tris-carborane thiol dendron or a hybrid dendron containing both PEG and carborane.

**Photochromic Properties of Polyoxotungstates with Grafted Spiropyran Molecules**

Arnaud Parrot, Guillaume Izzet,* Lise-Marie Chamoreau, Anna Proust, Olivier Oms, Anne Dolbecq, Khadija Hakouk, Houada El Bekkachi, Philippe Deniard, Rémi Dessapt,* and Pierre Mialane*

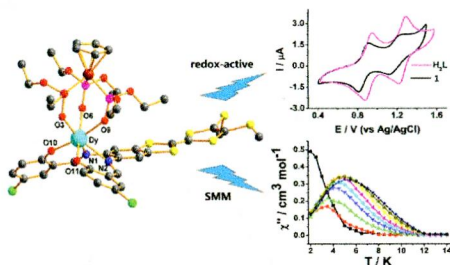
A new family of compounds, based on the covalent association of polyoxotungstates and spiropyrans, have been elaborated, and the influence of the inorganic moiety on the optical properties of the organic photochromic fragment(s) has been fully investigated both in solution and in the solid state.



Seven-Coordinate Lanthanide Sandwich-Type Complexes with a Tetrathiafulvalene-Fused Schiff Base Ligand

Feng Gao, Long Cui, Wei Liu, Liang Hu, Yu-Wu Zhong, Yi-Zhi Li, and Jing-Lin Zuo*

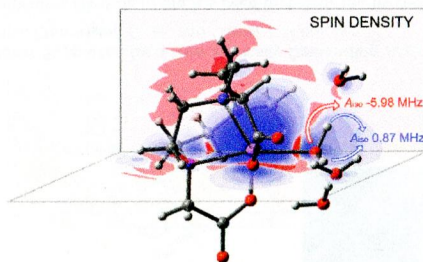
Three new seven-coordinate sandwich lanthanide(III) complexes, based on the tripodal ligand L_{OEt}^- and π -conjugated electrochemically active TTF-Schiff base ligand, have been synthesized and structurally characterized. Spectroscopic and electrochemical studies confirm their reversible redox properties. The Dy complex shows the field-induced SMM behavior. The results are helpful for further work on multifunctional molecular materials with intriguing structures and interesting physical properties.



Hyperfine Coupling Constants on Inner-Sphere Water Molecules of a Triazacyclononane-based Mn(II) Complex and Related Systems Relevant as MRI Contrast Agents

Véronique Patinec, Gabriele A. Rolla, Mauro Botta, Raphaël Tripier, David Esteban-Gómez, and Carlos Platas-Iglesias*

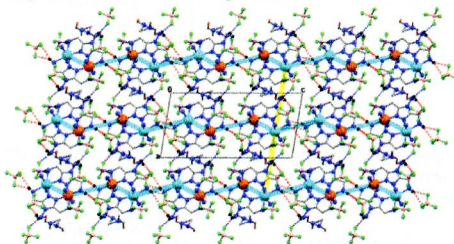
A combined ^1H and ^{17}O NMR relaxometric study of the $[\text{Mn}(\text{MeNO}_2\text{A})(\text{H}_2\text{O})]$ complex in combination with DFT calculations and molecular dynamics simulations within the atom-centered density matrix propagation (ADMP) approach was used to determine the ^1H and ^{17}O hyperfine coupling constants of the coordinated water molecule. This methodology was subsequently used to investigate different small Mn^{2+} complexes relevant as contrast agents in magnetic resonance imaging (MRI).



Effect of N^4 -Substituent Choice on Spin Crossover in Dinuclear Iron(II) Complexes of Bis-Terdentate 1,2,4-Triazole-Based Ligands

Jonathan A. Kitchen, Juan Olguin, Rafal Kulmaczewski, Nicholas G. White, Victoria A. Milway, Guy N. L. Jameson, Jeffery L. Tallon, and Sally Brooker*

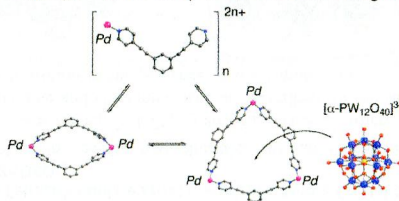
A general route to new 3,5-disubstituted 1,2,4-triazole ligands (here **PMRT**) in which the N^4 -substituent (**R**), off the “back” of the triazole, is systematically varied, along with the synthesis and full characterization of a family of seven $[\text{Fe}^{\text{II}}_2(\text{PMRT})_2](\text{BF}_4)_4$ ·solvent complexes, five of which are spin crossover active, from [HS–HS] to [HS–LS], is reported.



Synthesis and Characterization of Molecular Hexagons and Rhomboids and Subsequent Encapsulation of Keggin-Type Polyoxometalates by Molecular Hexagons

Kazuhiro Uehara, Takamichi Oishi, Takayuki Hirose, and Noritaka Mizuno*

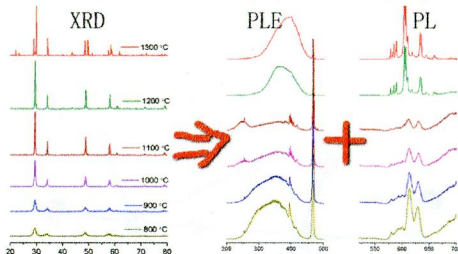
Structural control among hexagonal, rhomboidal, and infinite-chain supramolecular complexes with three different supporting ligands of ethylenediamine (**en**), N,N,N',N' -tetramethylethylenediamine (**en***), and 1,2-bis(diphenyl)phosphinoethane (**dppe**) $[(\text{en})\text{Pd}(\text{L})_3](\text{OTf})_6$ **1t**·**OTf**, $[(\text{en}^*)\text{Pd}(\text{L})_2](\text{PF}_6)_4$ **2d**·**PF**₆, and $[(\text{dppe})\text{Pd}(\text{L})](\text{OTf})_2$ **3**·**OTf** (**OTf** = trifluoromethane sulfonate; **L** = 1,3-bis(4-pyridylethynyl)benzene) in the solid and solution states was investigated. The addition of the highly negatively charged Keggin-type phosphododecatungstate $[\alpha\text{-PW}_{12}\text{O}_{40}]^{3-}$ to a solution of **2t/2d**·**PF**₆ resulted in the encapsulation of $[\alpha\text{-PW}_{12}\text{O}_{40}]^{3-}$ in the cavity of the molecular hexagon.



Wide-Band Excited $Y_6(WMo)_{0.5}O_{12}:Eu$ Red Phosphor for White Light Emitting Diode: Structure Evolution, Photoluminescence Properties, and Energy Transfer Mechanisms Involved

Huaiyong Li,* Hyeon Mi Noh, Byung Kee Moon, Byung Chun Choi, Jung Hyun Jeong,* Kiwan Jang, Ho Sueb Lee, and Soung Soo Yi

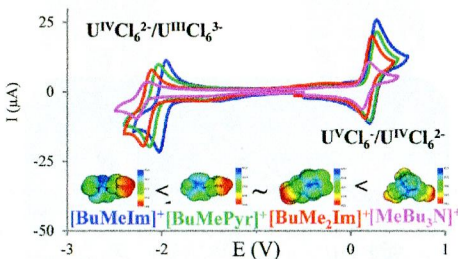
$Y_6(WMo)_{0.5}O_{12}$ activated with Eu^{3+} ions is a potential red-emitting conversion phosphor for WLEDs, which can be sensitized via host lattice as well as dopant. The symmetry and disorder of the host lattice strongly affect the excitation, energy transfer, and quenching processes, and therefore the photoluminescence properties of the phosphor.



Specific Interaction between Uranium Anionic Complexes and the Cations of Bis(trifluoromethylsulfonyl)imide Based Ionic Liquids

Céline Cannes,* Claire Le Naour, Philippe Moisy, and Philippe Guilbaud

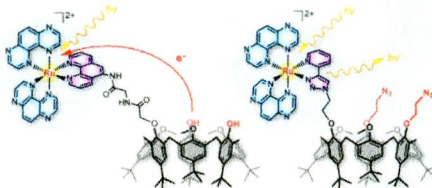
In $[Tf_2N]^-$ based ionic liquids, the cyclic voltammograms of uranium(IV) hexachloro complex present two redox couples: $U^VCl_6^{2-}/U^{IV}Cl_6^{2-}$ and $U^{IV}Cl_6^{2-}/U^{III}Cl_6^{3-}$. IL cations interact with the anionic uranium species. The magnitude of the ion pairing could be evaluated by voltammetry and ab initio calculations. The interaction increases with the charge of the uranium complex, $U^VCl_6^{2-} < U^{IV}Cl_6^{2-} < U^{III}Cl_6^{3-}$, and depends on the IL cation nature, $[MeBu_3N]^+ < [BuMe_2Im]^+ \approx [BuMePyr]^+ < [BuMeIm]^+$.



Synthesis and Electrochemical and Photophysical Properties of Calixarene-Based Ruthenium(II) Complexes as Potential Multivalent Photoreagents

Alice Mattiuzzi, Lionel Marcéls, Ivan Jabin,* Cécile Moucheron,* and Andrée Kirsch-De Mesmaeker*

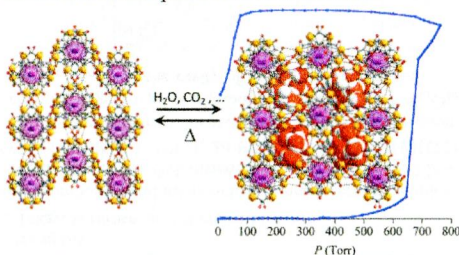
Calix[4 and 6]arenes functionalized by a $[\text{Ru}(\text{TAP})_2(\text{phen})]^{2+}$ or $[\text{Ru}(\text{TAP})_2(\text{pytz})]^{2+}$ complex give rise to intramolecular luminescence quenching by proton-coupled electron transfer because of the phenol groups, whereas the complex luminescence is restored when calix[6]arene contains azido instead of phenol arms.



Tetrahydrobenzoquinonate and Tetrachloranilate Zr(IV) Complexes: Single-Crystal-to-Single-Crystal Phase Transition and Open-Framework Behavior for $\text{K}_4\text{Zr}(\text{DBQ})_4$

Inhar Imaz, Georges Mouchaham, Nans Roques, Stéphane Brandès, and Jean-Pascal Sutter*

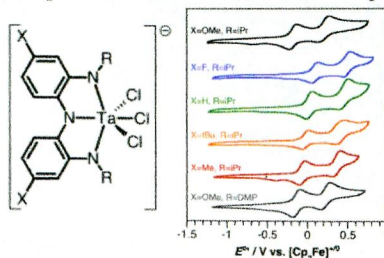
The preparation and crystal structures for $\text{K}_4[\text{Zr}(\text{DBQ})_4]$ and $\text{K}_4[\text{Zr}(\text{CA})_4]$, where DBQ^{2-} and CA^{2-} stand, respectively, for deprotonated dihydroxybenzoquinone and chloranilic acid, are described. In the solid state, $\text{K}_4[\text{Zr}(\text{DBQ})_4]$ exhibits a reversible close-to-open-framework transition in the presence of small molecules.



Tuning the Electronic and Steric Parameters of a Redox-Active Tris(amido) Ligand

Rui F. Munhá, Ryan A. Zarkesh, and Alan F. Heyduk*

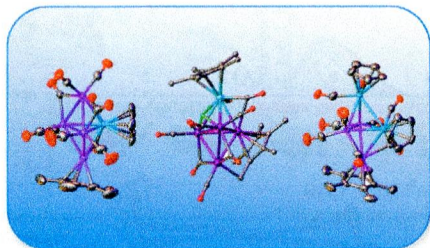
Redox-active tris(amido) ligands containing different electronic (X) and steric groups (R) are described. Tantalum complexes of the six ligand derivatives in each of three ligand oxidation states were prepared and then studied by a battery of structural, spectroscopic, and electrochemical techniques to elucidate the electronic and steric profiles manifested by each ligand.



Syntheses of Pentanuclear Group 6 Iridium Clusters by Core Expansion of Tetranuclear Clusters with $\text{Ir}(\text{CO})_2(\eta^5\text{-C}_5\text{Me}_4\text{R})$ ($\text{R} = \text{H, Me}$)

Michael D. Randles, Peter V. Simpson, Vivek Gupta, Junhong Fu, Graeme J. Moxey, Torsten Schwich, Alan L. Criddle, Simon Petrie, Jonathan G. MacLellan, Stuart R. Batten, Robert Stranger, Marie P. Cifuentes, and Mark G. Humphrey*

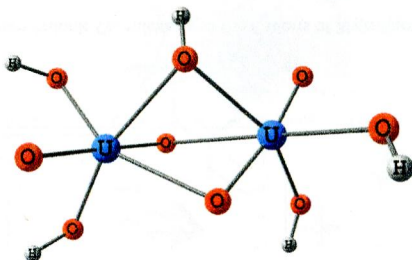
Mixed molybdenum/tungsten tetrairidium and dimolybdenum/ditungsten triiridium clusters were prepared in high yield by cluster-core expansion of molybdenum/tungsten triiridium and dimolybdenum/ditungsten diiridium precursors, respectively, and were analyzed by a combination of spectroscopic, structural, and theoretical techniques. Tetrahedral molybdenum/tungsten iridium mixed-metal clusters undergo cluster-core expansion with iridium capping reagents to afford trigonal-bipyramidal $\text{MIr}_4(\mu\text{-CO})_3(\text{CO})_7(\eta^5\text{-C}_5\text{H}_5)(\eta^5\text{-L}')$, $\text{MoIr}_4(\mu_3\text{-H})(\mu\text{-CO})_2(\mu\text{-}\eta^1\text{-}\eta^5\text{-CH}_2\text{C}_5\text{Me}_4)(\text{CO})_7(\eta^5\text{-C}_5\text{Me}_5)$ (possessing a $\mu\text{-}\eta^1\text{-}\eta^5\text{-CH}_2\text{C}_5\text{Me}_4$ ligand derived from a C–H bond activation of a C_5Me_5 methyl group), $\text{M}_2\text{Ir}_3(\mu\text{-CO})_3(\text{CO})_6(\eta^5\text{-C}_5\text{H}_5)_2(\eta^5\text{-L}')$, $\text{W}_2\text{Ir}_3(\mu\text{-CO})_4(\text{CO})_5(\eta^5\text{-C}_5\text{H}_5)_2(\eta^5\text{-C}_5\text{Me}_4\text{H})$, and $\text{Mo}_2\text{Ir}_3(\mu\text{-CO})_3(\text{CO})_6(\eta^5\text{-C}_5\text{Me}_5)_2$ ($\text{L}' = \text{C}_5\text{Me}_5, \text{C}_5\text{Me}_4\text{H}$). The spectroscopic, electrochemical, and spectroelectrochemical behavior of the clusters have been rationalized by time-dependent density functional theory.



Cation–Cation Interactions in $[(\text{UO}_2)_2(\text{OH})_n]^{4-n}$ Complexes

Samuel O. Odoh, Niranjana Govind, Georg Schreckenbach, and Wibe A. de Jong*

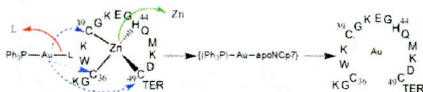
The structural and electronic properties of the $[(\text{UO}_2)_2(\text{OH})_n]^{4-n}$ ($n = 2\text{--}6$) series of complexes have been examined using density functional theory and correlated ab initio approaches. The lowest energy structure of $[(\text{UO}_2)_2(\text{OH})_5]^-$ possesses cation–cation interactions between the uranyl groups, in contrast to the situation in the complexes with 2, 4, and 6 hydroxo ligands.



Gold(I)-Phosphine-N-Heterocycles: Biological Activity and Specific (Ligand) Interactions on the C-Terminal HIVNCp7 Zinc Finger

Camilla Abbehausen, Erica J. Peterson, Raphael E. F. de Paiva, Pedro P. Corbi, André L. B. Formiga, Yun Qu, and Nicholas P. Farrell*

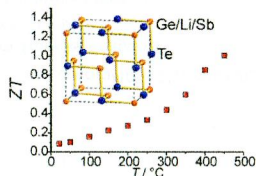
For the first time, Au(ligand) species (specifically $\{(PPh_3)Au\text{-apopetide}\}$) were observed upon reaction of Au(I) compounds with zinc finger peptides and Zn^{2+} ejection.



The Solid Solution Series $(GeTe)_x(LiSbTe_2)_2$ ($1 \leq x \leq 11$) and the Thermoelectric Properties of $(GeTe)_{11}(LiSbTe_2)_2$

Thorsten Schröder, Stefan Schwarz Müller, Christian Stiewe, Johannes de Boor, Markus Hölzel, and Oliver Oeckler*

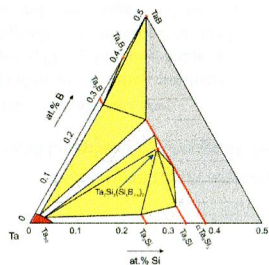
Exchanging one Ge^{2+} with two Li^+ per formula unit in $(GeTe)_n(Sb_2Te_3)$ ($n = 1, 2, 3, \dots$) eliminates cation vacancies, because it leads to an equal number of cations and anions. This substitution results in the solid solution $(GeTe)_x(LiSbTe_2)_2$ ($x = n - 1$), where Li acts as a "pseudo-vacancy". The thermoelectric properties of $(GeTe)_{11}(LiSbTe_2)_2$ show that this compound is a promising thermoelectric material with a ZT value of 1.0 at 450 °C.



Novel Refractory Phase, $Ta_7Si_2(Si_xB_{1-x})_2$

V. Romaka, V. Fosodeder, P. F. Rogli,* E. C. T. Ramos, C. A. Nunes, G. C. Coelho, and G. Giester

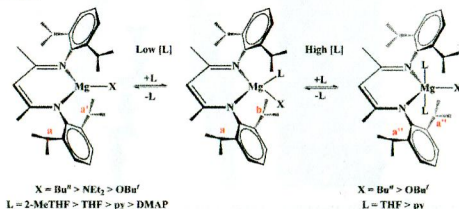
X-ray single crystal (XSC) and powder diffraction data (XPD) were used to elucidate the crystal structure of a new refractory silicon boride $Ta_7Si_2(Si_xB_{1-x})_2$ ($x = 0.12$). The architecture of the structure of $Ta_7Si_2(Si_xB_{1-x})_2$ combines layers of three-capped triangular metal prisms $(Si_xB)[Ta_{6i_2}(Si_xB)]$ alternating with double layers of two-capped $Si[Ta_{3i_1}Si]$ Archimedean metal antiprisms. Consequently, the metal framework contains (B/Si) pairs and $Si-Si$ dumbbells.



THF Exchange and Molecular Dynamics in the Series (BDI)MgX(THF), Where X = Buⁿ, NEt₂, and OBU^t and BDI = 2-[(2,6-Diisopropylphenyl)amino]-4-[(2,6-diisopropylphenyl)imino]pent-2-ene

Malcolm H. Chisholm,* Kittisak Choojun, Albert S. Chow, Gideon Fraenkel,* and Judith C. Gallucci

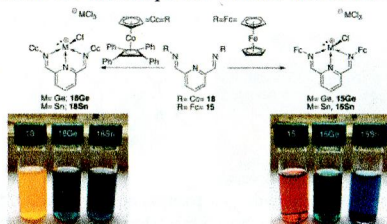
The complexes (BDI)MgX(THF), where X = Buⁿ, NEt₂, and OBU^t, are shown to undergo THF exchange at low added concentrations of THF by a dissociative mechanism. The apparent aryl group rotations involving the BDI ligands have the same activation parameters as the THF dissociation. The coalescence temperatures for apparent aryl group rotation, the dissociative exchange with added 2-MeTHF, the rotation about the Mg–O(THF) bond, and the reactivities of these complexes in solution are examined.



A Novel Diiminopyridine Ligand Containing Redox Active Co(III) Mixed Sandwich Complexes

Eleanor Magdzinski, Pierangelo Gobbo, Mark S. Workentin, and Paul J. Ragogna*

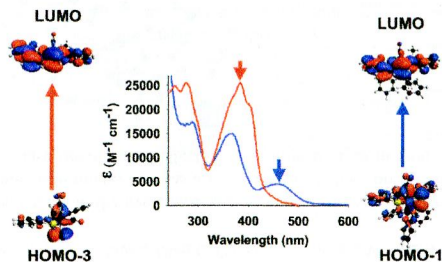
Main group compounds containing novel ligands with pendant redox active substituents have been synthesized. Electrochemical studies reveal a reversible two-electron process from the mixed sandwich cobaltocene moiety.



Photoactivity of Mono- and Dicarbonyl Complexes of Ruthenium(II) Bearing an N,N,S-Donor Ligand: Role of Ancillary Ligands on the Capacity of CO Photorelease

Margarita A. Gonzalez, Samantha J. Carrington, Indranil Chakraborty, Marilyn M. Olmstead, and Pradip K. Mascharak*

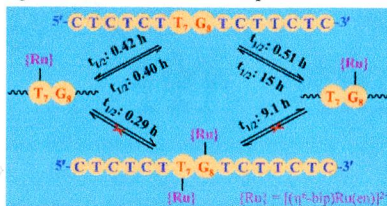
Mono- and dicarbonylruthenium complexes [Ru(Cl)(CO)(qmtpm)(PPh₃)]BF₄ (blue trace) and [Ru(Cl)(CO)₂(qmtpm)]-ClO₄ (red trace) readily release carbon monoxide (CO) upon illumination with light in the 300–500 nm range. Theoretical results confirm that metal-to-ligand charge-transfer transitions promote CO photorelease from these photoactive CO-releasing molecules.



Thymines in Single-Stranded Oligonucleotides and G-Quadruplex DNA Are Competitive with Guanines for Binding to an Organoruthenium Anticancer Complex

Kui Wu, Suyan Liu, Qun Luo, Wenbing Hu, Xianchan Li, Fuyi Wang,* Renhui Zheng, Jie Cui, Peter J. Sadler,* Junfeng Xiang, Qiang Shi, and Shaoliang Xiong

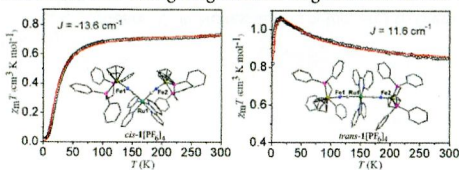
The thymines in the middle region (T₇/T₁₁ or T₆/T₁₁) of single-stranded oligodeoxynucleotides 5'-CTCTCTX₇G₈Y₉CTTCTC-3' [X, Y = T, C, or A] are kinetically competitive with guanine for binding to [(η⁶-arene)Ru(en)Cl]⁺ (I). More importantly, the T bases in the loops of telomeric G-quadruplex DNA are found to be more competitive both kinetically and thermodynamically with G bases for binding to I. These suggest that thymines play a unique role in the ruthenation of DNA by organoruthenium anticancer complexes.



From Antiferromagnetic to Ferromagnetic Interaction in Cyanido-Bridged Fe(III)–Ru(II)–Fe(III) Complexes by Change of the Central Diamagnetic Cyanido-Metal Geometry

Xiao Ma, Sheng-Min Hu, Chun-Hong Tan, Yong-Fan Zhang,* Xu-Dong Zhang, Tian-Lu Sheng,* and Xin-Tao Wu

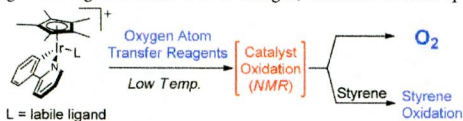
The first example of the *cis*-/*trans*-isomer with multistates, *cis*-/*trans*-1[PF₆]₂, and their two-electron-oxidation products, *cis*-/*trans*-1[PF₆]₄, have been synthesized and structurally characterized. Moreover, for *cis*-/*trans*-1[PF₆]₄, the long-distance magnetic interactions on the geometry effects of the diamagnetic cyanidometal bridging ligands were investigated. DFT calculations were performed to rationalize their strong long-distance magnetic interactions and their magnetic differences.



Probing the Oxidation Chemistry of Half-Sandwich Iridium Complexes with Oxygen Atom Transfer Reagents

Christopher R. Turlington, Daniel P. Harrison, Peter S. White, Maurice Brookhart, and Joseph L. Templeton*

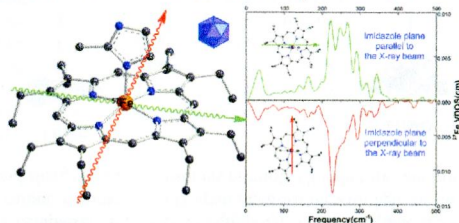
Oxidation of half-sandwich Cp* iridium complexes related to water oxidation catalysts with iodobenzene or dimethyldioxirane at low temperatures resulted in either decomposition to acetic acid or formation of heterogeneous particles or paramagnetic species, respectively. No Ir(V)oxo complex was observed. In separate experiments, a Cp* iridium hydride complex was found to extract Ag⁺ from AgCl to form a silver-bridged, dinuclear iridium species.



Probing Heme Vibrational Anisotropy: An Imidazole Orientation Effect?

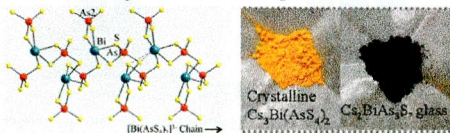
Qian Peng, Ming Li, Chuanjiang Hu, Jeffrey W. Pavlik, Allen G. Oliver, E. Ercan Alp, Michael Y. Hu, Jiyong Zhao, J. Timothy Sage,* and W. Robert Scheidt*

The oriented single-crystal iron vibrations in the five-coordinate high-spin iron(II) porphyrinate [Fe(OEP)(2-MeHIm)] have been examined by NRVs. The imidazole orientation has a relatively small effect on the in-plane iron motion, but the more strongly bonded imidazolite does have orientational effects on the in-plane iron motion.

**Crystalline and Glassy Phases in the Cs/Bi/As/S System**

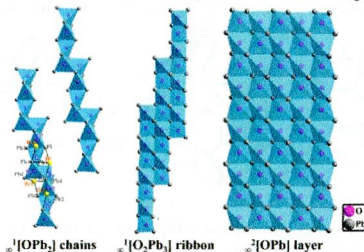
Tarun K. Bera, Ratnasabapathy G. Iyer, Christos D. Malliakas, and Mercuri G. Kanatzidis*

The tuning of the polysulfide flux basicity dictates the thioarsenate fragments in the final products. High basicity leads to crystalline [As^VS₄]³⁻-containing compounds Cs₃Bi(AsS₄)₂ and Cs₃Bi(AsS₄)₄, whereas lower basicity stabilizes a series of novel glasses of the formula Cs_{n-1}BiAs_nS_{2n+1} containing the reduced As^{III} species.

**Special ∞^1 [OPb₂] Chains and ∞^1 [O₂Pb₃] Ribbons Based on OPb₄ Anion-Centered Tetrahedra in Pb₂(O₄Pb₈)(BO₃)₃Br₃ and Pb₂(O₈Pb₁₂)(BO₃)₂Br₆**

Lingyun Dong, Shilie Pan,* Ying Wang, Hongwei Yu, Xiaoyu Dong, Shujuan Han, and Min Zhang*

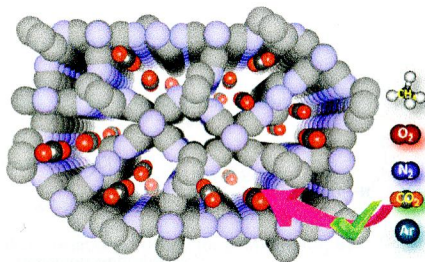
Two Br atoms are attached to the chains at the opposite position rotating the two pairs of edge-sharing OPb₄ tetrahedra, while the other type of Br atoms do not play the role of rotation, resulting in the ∞^1 [OPb₂] chains constructed by finite linear zweier chains via the opposite edges in Pb₂(O₄Pb₈)(BO₃)₃Br₃. The chains in Pb₂(O₄Pb₈)(BO₃)₃Br₃ and ribbons in Pb₂(O₈Pb₁₂)(BO₃)₂Br₆ can be viewed as derivatives from the tetrahedral layer observed in tetragonal PbO compound.



Effect of Pillar Modules and Their Stoichiometry in 3D Porous Frameworks of Zn(II) with $[\text{Fe}(\text{CN})_6]^{3-}$: High CO_2/N_2 and CO_2/CH_4 Selectivity

Arpan Hazra, Satyanarayana Bonakala, Sandeep K. Reddy, Sundaram Balasubramanian,* and Tapas Kumar Maji*

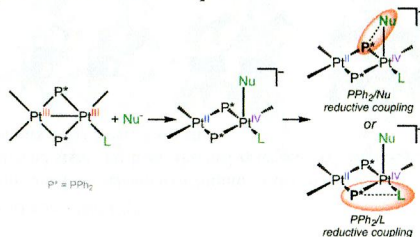
Three 3D metal–organic frameworks have been assembled by the reaction of Zn(II), $[\text{Fe}(\text{CN})_6]^{3-}$, and 4,4'-bipyridyl/4,4'-azobipyridyl linkers. The frameworks show selective CO_2 adsorption over N_2 , CH_4 , Ar, and O_2 and exhibit good CO_2 selectivity over N_2 and CH_4 at 273 K. The high values of ΔH_{CO_2} and ΔH_{H_2} stem from the preferential electrostatic interaction of CO_2 with the unsaturated metal sites, pendent nitrogen atoms of $[\text{Fe}(\text{CN})_6]^{3-}$, and π -electron cloud of bipyridine aromatic rings.



Addition of Nucleophiles to Phosphanido Derivatives of Pt(III): Formation of P–C, P–N, and P–O Bonds

Andersson Arias, Juan Forniés, Consuelo Fortuño,* Susana Ibáñez, Antonio Martín, Piero Mastrolilli,* Vito Gallo, and Stefano Todisco

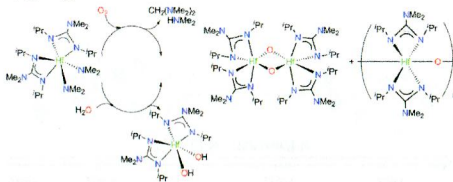
Coordination of a nucleophile to a square planar platinum(III) center is a way to induce a reductive coupling between a diphenylphosphanido bridging ligand and the added nucleophile.



Reactions of Group 4 Amide Guanidates with Dioxigen or Water. Studies of the Formation of Oxo Products

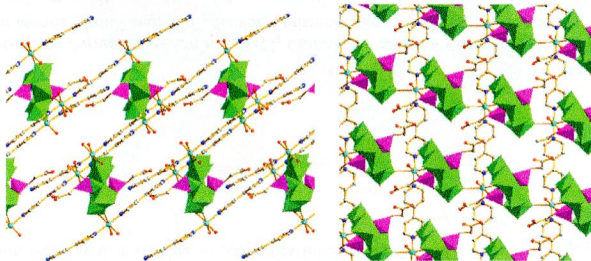
Bhavna Sharma, Tabitha M. Callaway, Adam C. Lamb, Carlos A. Steren, Shu-Jian Chen, and Zi-Ling Xue*

Reactions of amide guanidates with O_2 or H_2O have recently been used to make metal oxides into microelectronic materials. The reaction of $(Me_2N)_2Hf[{}^iPrNC(NMe_2)N{}^iPr]_2$ with O_2 or H_2O gives the oxo dimer $\{Hf(\mu-O)[{}^iPrNC(NMe_2)N{}^iPr]_2\}_2$ and polymer $\{Hf(\mu-O)[{}^iPrNC(NMe_2)N{}^iPr]_2\}_n$. Mass spectrometric analysis of the reaction with water in air shows formation of the oxo dimer and dihydroxyl $Hf(OH)_2[{}^iPrNC(NMe_2)N{}^iPr]_2$. Kinetic studies of the reaction with 1.0 atm of O_2 show that it follows pseudo-first-order kinetics, giving ΔH^\ddagger and ΔS^\ddagger .

**Functionalized Pentamolybdo(diphosphate)-Based Inorganic–Organic Hybrids: Synthesis, Structure, and Properties**

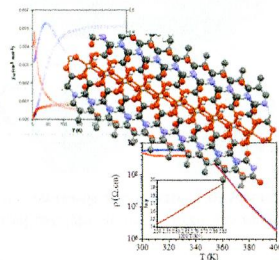
Xiao-Min Li, Ya-Guang Chen,* Chunnian Su, Shi Zhou, Qun Tang, and Tian Shi

Three inorganic–organic hybrids based on a functionalized pentamolybdo(diphosphate) anion $[(HO_2CC_2H_4PO_3)_2Mo_5O_{15}]^{4-}$ have been synthesized at different pH values with conventional method. In compound **1**, $[(HO_2CC_2H_4PO_3)_2Mo_5O_{15}]^{4-}$ acts as a tridentate ligand and coordinates to the Co^{2+} ions of trimeric complex cations $[Co_3(bipy)_4(H_2O)_6]^{6+}$ forming a complex layer. In **3** $[(HO_2CC_2H_4PO_3)_2Mo_5O_{15}]^{4-}$ acts as a bidentate ligand and coordinates to the Cu^{2+} ions of complex chains $[Cu(bipy)(H_2O)_2]^{2+}$, forming a different layer from that in **1**.

**Semiconductive and Magnetic One-Dimensional Coordination Polymers of Cu(II) with Modified Nucleobases**

Pilar Amo-Ochoa,* Oscar Castillo, Carlos J. Gómez-García, Khaled Hassanein, Sandeep Verma,* Jitendra Kumar, and Félix Zamora*

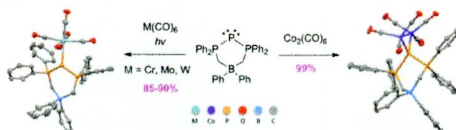
$[Cu(TAcO)_2(H_2O)_2]_n$, $[Cu_{1.5}(TAcO)_2(H_2O)(OH)]_n \cdot 4H_2O$, and $[Cu_3(UPrO)_2Cl_2(OH)_2(H_2O)_2]_n$ are coordination polymers containing modified nucleobases as ligands showing semiconductor and magnetic properties. Three coordination polymers of copper(II) with thymine-1-acetic acid and uracil-1-propionic carboxylate as ligands, $[Cu(TAcO)_2(H_2O)_2]_n$, $[Cu_3(TAcO)_4(H_2O)_2(OH)_2]_n \cdot 4H_2O$, and $[Cu_3(UPrO)_2Cl_2(OH)_2(H_2O)_2]_n$ ($TAcOH$ = thymine-1-acetic acid, $UPrOH$ = uracil-1-propionic acid), have been prepared and structurally characterized. Their physical properties show unprecedented coexistence of semiconductor and magnetic properties for this type of compound.



Synthesis of Zwitterionic Triphosphenium Transition Metal Complexes: A Boron Atom Makes The Difference

Jonathan W. Dube, Charles L. B. Macdonald, Bobby D. Ellis, and Paul J. Ragogna*

A series of zwitterionic phosphorus(I) metal carbonyl complexes was synthesized in excellent yields with structures confirmed crystallographically, representing the first such examples of this old family of compounds to be isolated and structurally authenticated. One lone pair is utilized in bonding the $M(\text{CO})_5$ ($M = \text{Cr}, \text{Mo}, \text{W}$; left), while the $\text{Co}_2(\text{CO})_6$ metal complex (right) is a rare example of simultaneous donation of both lone pairs of electrons on the P(I) center. The anionic borate backbone (blue atom) proves to be critical in isolating these species as the analogous cationic triphosphenium ions generate metal complexes that are unstable.



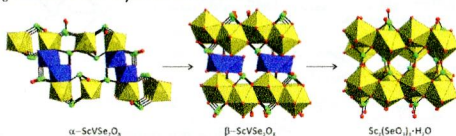
11450 5

dx.doi.org/10.1021/ic401769s

α -ScVSe₂O₈, β -ScVSe₂O₈, and ScVTe₂O₈: New Quaternary Mixed Metal Oxides Composed of Only Second-Order Jahn–Teller Distortive Cations

Yeong Hun Kim, Dong Woo Lee, and Kang Min Ok*

A series of new quaternary scandium vanadium selenium/tellurium oxides materials, α -ScVSe₂O₈, β -ScVSe₂O₈, and ScVTe₂O₈ have been synthesized by standard solid-state and hydrothermal reactions. While α -ScVSe₂O₈ and β -ScVSe₂O₈ exhibit 3D framework structures, ScVTe₂O₈ shows a 2D layered structure.



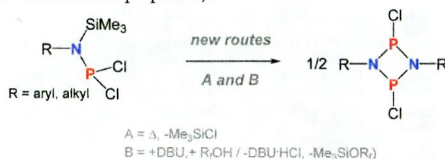
11457 5

dx.doi.org/10.1021/ic401772h

Synthesis of 1,3-Dichloro-*cyclo*-1,3-diphosphadiazanes from Silylated Amino(dichloro)phosphanes

Axel Schulz,* Alexander Villinger, and Andrea Westenkirchner

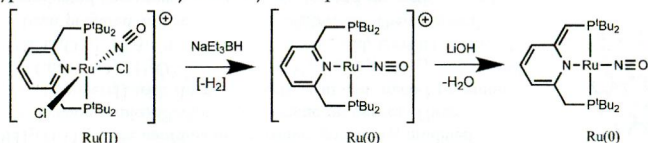
In a systematic study the synthesis of differently substituted 1,3-dichloro-*cyclo*-1,3-diphosphadiazanes [$\text{CIP}(\mu\text{-NR})_2$] was achieved by thermal elimination of Me_3SiCl from silylated amino(dichloro)phosphanes, $\text{R-N}(\text{SiMe}_3)\text{P}(\text{Cl})_2$, and/or by adding a mixture of $\text{R}_2\text{OH}/\text{base}$ ($\text{R}_2\text{OH} = \text{hexafluoroisopropanol}$).



Ru(0) and Ru(II) Nitrosyl Pincer Complexes: Structure, Reactivity, and Catalytic Activity

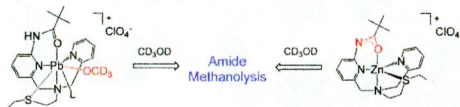
Eran Fogler, Mark A. Iron, Jing Zhang, Yehoshua Ben-David, Yael Diskin-Posner, Gregory Leitus, Linda J. W. Shimon, and David Milstein*

Despite considerable interest in ruthenium carbonyl pincer complexes and their substantial catalytic activity, there has been relatively little study of the isoelectronic ruthenium nitrosyl complexes. Here we describe the synthesis and reactivity of several complexes of this type as well as the catalytic activity of complex 6.

**Pb(II)-Promoted Amide Cleavage: Mechanistic Comparison to a Zn(II) Analogue**

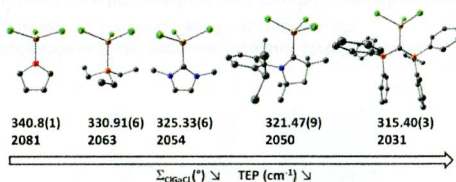
Eric S. Elton, Tingting Zhang, Rajeev Prabhakar, Atta M. Arif, and Lisa M. Berreau*

The influence of Pb(II) on an amide methanolysis reaction has been evaluated by comparative kinetic, thermodynamic, mechanistic, and computational studies with a Zn(II) analogue. While both metal ions promote amide cleavage, differences are found within the reaction pathway that are due to properties inherent to the Pb(II) ion.

**Relationship between Gallium Pyramidalization in L-GaCl₃ Complexes and the Electronic Ligand Properties**

Ahmad El-Hellani, Julien Monot, Shun Tang, Régis Guillot, Christophe Bour, and Vincent Gandon*

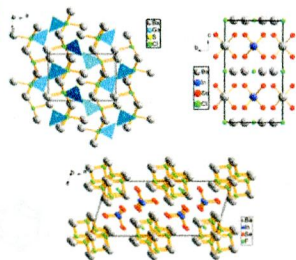
New adducts of GaCl_3 with strong donor ligands of the carbon(0) and CAAC series have been synthesized and characterized by X-ray crystallography. The exceptional pyramidalization of the GaCl_3 moiety compared to other complexes raised the question whether a correlation could be established between the sum of the $\text{Cl}-\text{Ga}-\text{Cl}$ angles and electronic properties of the ligand. A gallium-scale based on the solid state structures has been established and compared to the Tolman Electronic Parameter.



Five New Chalcogenides, $\text{Ba}_3\text{GaS}_4\text{X}$ ($\text{X} = \text{Cl}, \text{Br}$), $\text{Ba}_3\text{MSe}_4\text{Cl}$ ($\text{M} = \text{Ga}, \text{In}$), and $\text{Ba}_7\text{In}_2\text{Se}_6\text{F}_8$: Syntheses, Crystal Structures, and Optical Properties

Kai Feng, Wenlong Yin, Zuohong Lin, Jiyong Yao,* and Yicheng Wu

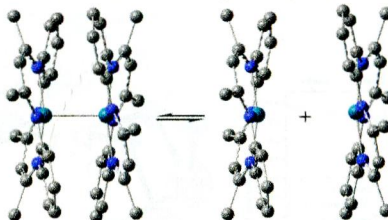
A new series of chalcogenides, $\text{Ba}_3\text{GaS}_4\text{X}$ ($\text{X} = \text{Cl}, \text{Br}$), $\text{Ba}_3\text{MSe}_4\text{Cl}$ ($\text{M} = \text{Ga}, \text{In}$) and $\text{Ba}_7\text{In}_2\text{Se}_6\text{F}_8$ have been obtained. $\text{Ba}_3\text{GaS}_4\text{X}$ ($\text{X} = \text{Cl}, \text{Br}$) and $\text{Ba}_3\text{MSe}_4\text{Cl}$ ($\text{M} = \text{Ga}, \text{In}$) contain different kinds of pseudolayer structures, while $\text{Ba}_7\text{In}_2\text{Se}_6\text{F}_8$ possesses unique one-dimensional structure. $\text{Ba}_3\text{GaQ}_4\text{X}$ ($\text{Q} = \text{S}, \text{X} = \text{Cl}, \text{Br}$; $\text{Q} = \text{Se}, \text{X} = \text{Cl}$) possess band gaps of 2.14, 1.80, and 2.05 eV, respectively.



Evaluation of the $\text{Rh}^{\text{III}}-\text{Rh}^{\text{III}}$ Bond Dissociation Enthalpy for $[(\text{TMTAA})\text{Rh}]_2$ by ^1H NMR T_2 Measurements: Application in Determining the $\text{Rh}-\text{C}(\text{O})-$ BDE in $[(\text{TMTAA})\text{Rh}]_2\text{C}=\text{O}$

Gregory H. Immler, Michael J. Zdzilla,* and Bradford B. Wayland*

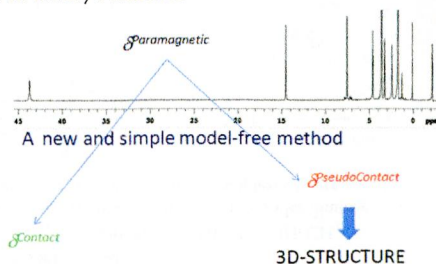
Temperature dependence of the rates of $\text{Rh}^{\text{II}}-\text{Rh}^{\text{II}}$ dissociation give the activation parameters for bond homolysis $\Delta H_{\text{app}}^\ddagger = 24(1) \text{ kcal mol}^{-1}$ and $\Delta S_{\text{app}}^\ddagger = 10(1) \text{ cal K}^{-1} \text{ mol}^{-1}$ and an estimate for the $\text{Rh}^{\text{II}}-\text{Rh}^{\text{II}}$ bond dissociation enthalpy of 22 kcal mol^{-1} . Thermodynamic values for reaction of **1** with CO to form $(\text{TMTAA})\text{Rh}-\text{C}(\text{O})-\text{Rh}(\text{TMTAA})$ (**3**) $\Delta H_1^\circ = -14(1) \text{ kcal mol}^{-1}$, $\Delta S_1^\circ = -30(3) \text{ cal K}^{-1} \text{ mol}^{-1}$ were used in deriving a $(\text{TMTAA})\text{Rh}-\text{C}(\text{O})-$ BDE of 53 kcal mol^{-1} .



A Simple and General Method to Determine Reliable Pseudocontact Shifts in Lanthanide Complexes

Roberto Berardozi and Lorenzo Di Bari*

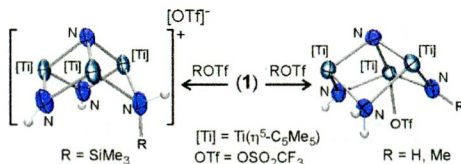
Lanthanide pseudocontact shifts (PCS) make paramagnetic NMR one of the most accurate methods for solution structures. PCS are commonly obtained from total paramagnetic shifts through linearization methods, which rely on (a) isostructurality and (b) the validity of Bleaney's constants. We generalize and demonstrate a method we recently proposed that does not rely on any structural hypothesis nor on Bleaney's constants.



Reactivity with Electrophiles of Imido Groups Supported on Trinuclear Titanium Systems

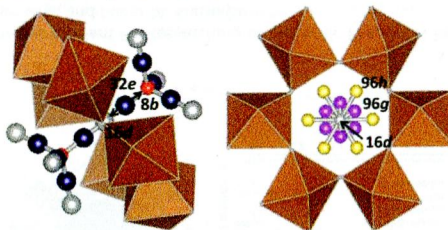
Jorge Caballo, Mariano González-Moreiras, Miguel Mena, Adrián Pérez-Redondo, and Carlos Yélamos*

The electrophilic attack of ROTf (R = H, Me) on $[\{\text{Ti}(\eta^5\text{-C}_5\text{Me}_5)(\mu\text{-NH})\}_3(\mu_3\text{-N})]$ (**1**) occurs at one NH imido ligand to give $[\text{Ti}_3(\eta^5\text{-C}_5\text{Me}_5)_3(\mu_3\text{-N})(\mu\text{-NH})_2(\mu\text{-NHR})(\text{OTf})]$ derivatives, which undergo rearrangement reactions involving triflate-assisted proton exchange between amido NHR and imido NH ligands. The larger trimethylsilyl fragment of Me_3SiOTf attacks the same nitrogen of **1** but produces a complex $[\text{Ti}_3(\eta^5\text{-C}_5\text{Me}_5)_3(\mu_3\text{-N})(\mu\text{-NH})_2(\mu\text{-NHSiMe}_3)][\text{OTf}]$ with the triflate anion not coordinated to the metals.

**Structural Investigation of the Substituted Pyrochlore AgSbO_3 through Total Scattering Techniques**

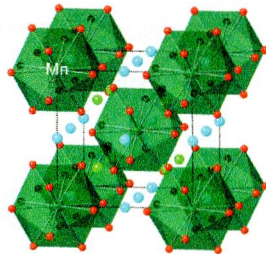
Geneva Laurita, Katharine Page, A. W. Sleight, and M. A. Subramanian*

Polycrystalline samples of the pyrochlore series $\text{Ag}_{1-x}\text{M}^x\text{SbO}_{3+x[(n-1)/2]}$ ($\text{M} = \text{Na}, \text{K}, \text{ and } \text{Tl}$) have been structurally analyzed through total scattering techniques. The upper limits of x obtained were 0.05 for Na, 0.16 for K, and 0.17 for Tl. The Ag^+ cation occupies a site with inversion symmetry on a 3-fold axis.

**A-Site-Ordered Perovskite $\text{MnCu}_3\text{V}_4\text{O}_{12}$ with a 12-Coordinated Manganese(II)**

Yasuhide Akizuki, Ikuya Yamada,* Koji Fujita,* Norimasa Nishiyama, Tetuo Irifune, Takeshi Yajima, Hiroshi Kageyama, and Katsuhisa Tanaka

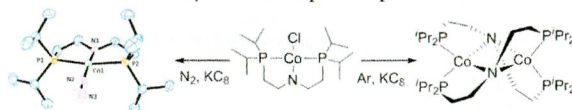
A novel cubic perovskite $\text{MnCu}_3\text{V}_4\text{O}_{12}$ has been synthesized at a high pressure and high temperature of 12 GPa and 1373 K. This compound crystallizes in the A-site-ordered perovskite structure (space group $\text{Im}\bar{3}$) with lattice constant $a = 7.26684(10)$ Å at room temperature.



Chemistry of Reduced Monomeric and Dimeric Cobalt Complexes Supported by a PNP Pincer Ligand

Sergio S. Rozenel, Rosa Padilla, and John Arnold*

The reduction chemistry of cobalt complexes with HPNP (HPNP = $\text{HN}(\text{CH}_2\text{CH}_2\text{P}^i\text{Pr}_2)_2$) as a supporting ligand is described. Monomeric square planar $[(\text{PNP})\text{CoN}_2]$ is obtained by reduction under dinitrogen, whereas dimeric $[(\text{PNP})\text{Co}]_2$ is formed under argon. The one- and two-electron reactivity of these complexes is presented.

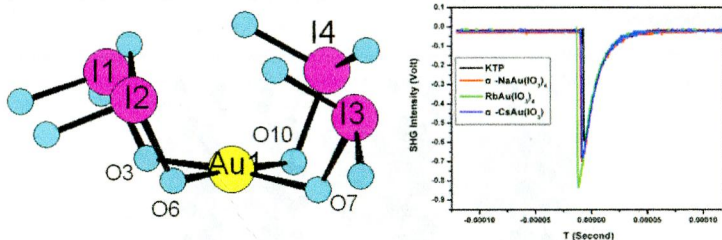
**11551 **5****

dx.doi.org/10.1021/ic401891f

Explorations of a Series of Second Order Nonlinear Optical Materials Based on Monovalent Metal Gold(III) Iodates

Chao Huang, Chun-Li Hu, Xiang Xu, Bing-Ping Yang, and Jiang-Gao Mao*

A series of monovalent metal gold(III) iodates containing $\text{Au}(\text{IO}_3)_4^-$ anions have been reported, among which $\alpha\text{-NaAu}(\text{IO}_3)_4$, $\text{RbAu}(\text{IO}_3)_4$, and $\alpha\text{-CsAu}(\text{IO}_3)_4$ display moderate strong SHG responses of 1.17 \times , 1.33 \times , and 1.17 \times KTP, respectively, and all of them are type-I phase-matchable.

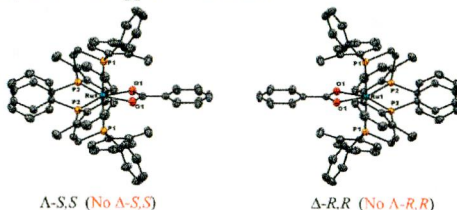
**11563 **5****

dx.doi.org/10.1021/ic401908t

Chiral Induction at Octahedral Ru(II) via the Disassembly of Diruthenium(II,III) Tetracarboxylates Using a Variety of Chiral Diphosphine Ligands

Brandon R. Groves, D. Ian Ar buckle, Ernest Essoun, Travis L. Lundrigan, Ruiyao Wang, and Manuel A. S. Aquino*

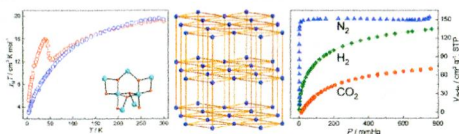
Very high diastereoselectivity was maintained when a tetrahedral to octahedral chiral induction methodology, involving the disassembly of diruthenium(II,III) tetracarboxylates with chiral diphosphines, was extended to include (1) larger carboxylates, (2) chirality at the two phosphine centers, and (3) single site chirality between the P-atoms. X-ray crystallography, solution and solid-state circular dichroism, and NMR support the conclusions.



Four Coordination Polymers Based on Identical Eight-Connected Heptanuclear Clusters: Spin Canting, Spin Glass, Antiferromagnetism, and Gas Adsorption

Jia Li, Bao Li, Peng Huang, Hai-Yan Shi,* Rong-Bin Huang, Lan-Sun Zheng, and Jun Tao*

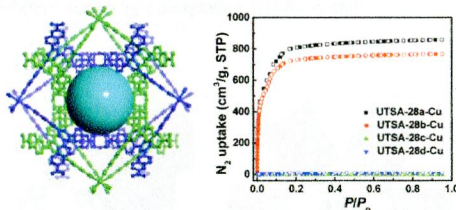
Four coordination polymers with identical heptanuclear metal clusters showing diverse magnetic properties and H₂ and CO₂ uptake capacities are reported.



Metastable Interwoven Mesoporous Metal–Organic Frameworks

Yabing He,* Zhiyong Guo, Shengchang Xiang, Zhangjing Zhang, Wei Zhou, Frank R. Fronczek, Sean Parkin, Stephen T. Hyde, Michael O’Keeffe, and Banglin Chen*

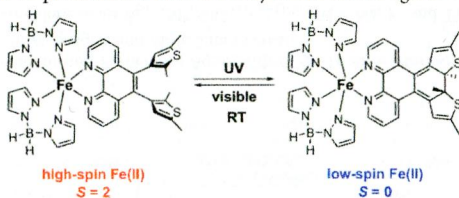
A series of interwoven mesoporous metal–organic frameworks were structurally characterized and examined for their gas sorption, underlying their metastable structure feature.



Spin Crossover Meets Diarylethenes: Efficient Photoswitching of Magnetic Properties in Solution at Room Temperature

Magdalena Milek, Frank W. Heinemann, and Marat M. Khusniyarov*

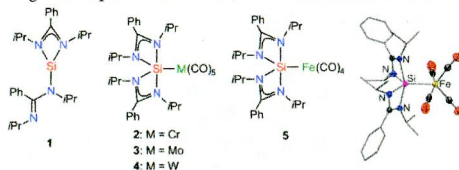
Reversible photoswitching between paramagnetic high-spin and diamagnetic low-spin states of an iron(II) complex is achieved at room temperature in solution via photoisomerization of a diarylethene-derived ligand.



Five-Coordinate Silicon(II) Compounds with Si–M Bonds (M = Cr, Mo, W, Fe): Bis(*N,N'*-diisopropylbenzamidinato(–))silicon(II) as a Ligand in Transition-Metal Complexes

Konstantin Junold, Johannes A. Baus, Christian Burschka, Thomas Vent-Schmidt, Sebastian Riedel,* and Reinhold Tacke*

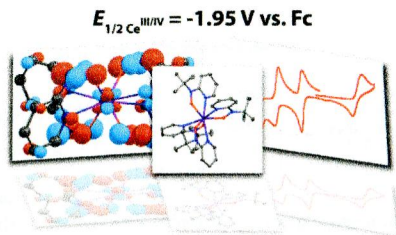
Reaction of the donor-stabilized silylene **1** with $[\text{Cr}(\text{CO})_6]$, $[\text{Mo}(\text{CO})_6]$, $[\text{W}(\text{CO})_6]$, or $[\text{Fe}(\text{CO})_5]$ leads to the formation of the transition-metal silylene complexes **2–5**, which contain five-coordinate silicon(II) moieties with Si–M bonds (M = Cr, Mo, W, Fe). These compounds were characterized by NMR spectroscopic studies in the solid state and in solution and by crystal structure analyses. According to computational studies, the Si–M bonds are best described as single bonds.



Homoleptic Cerium(III) and Cerium(IV) Nitroxide Complexes: Significant Stabilization of the 4+ Oxidation State

Justin A. Bogart, Andrew J. Lewis, Scott A. Medling, Nicholas A. Piro, Patrick J. Carroll, Corwin H. Booth, and Eric J. Schelter*

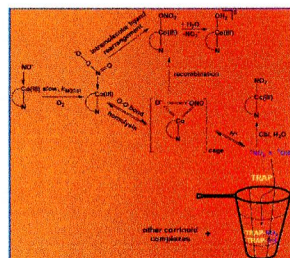
Strongly electron-donating nitroxide ligands confer significant stability to Ce in the 4+ oxidation state. Electrochemical measurements reveal a shift in the reduction potential of +2.51 V for the potential for $[\text{Bu}_4\text{N}]_2[\text{Ce}(\text{NO}_3)_6]$ in acetonitrile. Density functional theory calculations support symmetry-allowed donation of filled ligand orbitals into vacant metal 4f orbitals as a basis for this stabilization.



Mechanistic Studies on the Reaction of Nitroxy cobalamin with Dioxygen: Evidence for Formation of a Peroxynitritocob(III) alamin Intermediate

Harishchandra Subedi and Nicola E. Brasch*

A detailed mechanistic investigation of the oxidation of NOCbl by oxygen is presented. Only base-on NOCbl reacts with O_2 , and the reaction proceeds via an associative mechanism involving a peroxynitritocob(III)alamin intermediate, $\text{Co}(\text{III})\text{-N}(\text{O})\text{OO}^\cdot$. The intermediate undergoes O–O bond homolysis and ligand isomerization to ultimately yield NO_2Cbl and $\text{H}_2\text{OCbl}^+/\text{HOCbl}$, respectively. Formation of $^\bullet\text{OH}$ and $^\bullet\text{NO}_2$ intermediates from O–O bond homolysis is demonstrated using trapping agents and the characterization of a corrinoid product with minor corrin ring modifications.



Synthesis, Structural Characterization, and Electrochemical Properties of Dinuclear Ni/Mn Model Complexes for the Active Site of [NiFe]-Hydrogenases

Li-Cheng Song,* Jia-Peng Li, Zhao-Jun Xie, and Hai-Bin Song

The first neutral Ni/Mn model complexes with a novel triply bridged dinuclear core $[\text{Ni}(\mu\text{-S})_2(\mu\text{-X})\text{Mn}]$ ($\text{X} = \text{Cl}, \text{Br}$) have been synthesized and structurally characterized. Some of them have been found to be catalysts for proton reduction to give hydrogen under electrochemical conditions.

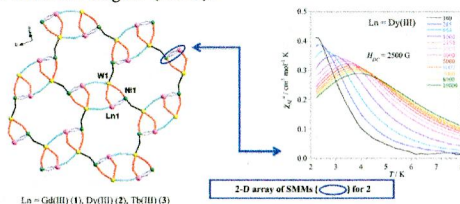


The prepared Ni/Mn model complexes as electrocatalysts to produce H_2

Two-Dimensional Coordination Polymers Constructed by $[\text{Ni}^{\text{II}}\text{Ln}^{\text{III}}]$ Nodes and $[\text{W}^{\text{IV}}(\text{bpy})(\text{CN})_6]^{2-}$ Spacers: A Network of $[\text{Ni}^{\text{II}}\text{Dy}^{\text{III}}]$ Single Molecule Magnets

Maria-Gabriela Alexandru, Diana Visinescu, Sergiu Shova, Francesc Lloret, Miguel Julve,* and Marius Andruh*

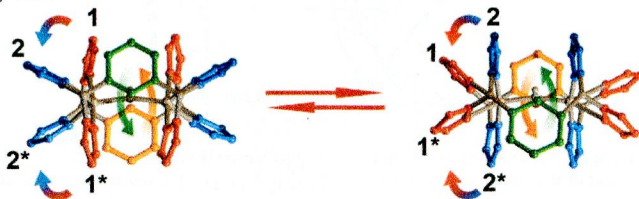
Three isomorphous two-dimensional (2D) coordination polymers of general formula $\{[\text{Ni}^{\text{II}}(\text{valpn})\text{Ln}^{\text{III}}(\text{NO}_3)(\text{H}_2\text{O})(\mu\text{-NC})_4\text{W}^{\text{IV}}(\text{bpy})(\text{CN})_2] \cdot x\text{H}_2\text{O} \cdot y\text{CH}_3\text{CN}\}_n$, have been synthesized by reacting $\text{Ph}_4\text{P}[\text{W}^{\text{V}}(\text{CN})_6(\text{bipy})]$ with the heterodinuclear $[\text{Ni}^{\text{II}}\text{Ln}^{\text{III}}(\text{valpn})(\text{O}_2\text{NO})_3]$ complexes [$\text{H}_2\text{valpn} = 1,3\text{-propanediyl-bis}(2\text{-iminomethylene-6-methoxyphenol})$, $\text{bipy} = 2,2'\text{-bipyridine}$, and $\text{Ln} = \text{Gd}$ (1), Dy (2), and Tb (3) with $x = 2$ (1), 3.9 (2), and 3.35 (3) and $y = 2.50$ (1), 2 (2), and 1.8 (3)]. Their crystal structures consist of $[\text{Ni}^{\text{II}}\text{Ln}^{\text{III}}]$ 3d-4f nodes which are connected by $[\text{W}^{\text{IV}}(\text{bpy})(\text{CN})_6]^{2-}$ diamagnetic linkers resulting from the reduction of W^{V} to W^{IV} during the reaction process. The $\text{Dy}(\text{III})$ derivative represents the first example of a 2D 3d-4f heterobimetallic single molecule magnet (SMM).



Zinc(II) and Cadmium(II) Monohydroxide Bridged, Dinuclear Metallacycles: A Unique Case of Concerted Double Berry Pseudorotation

Daniel L. Reger,* Andrea E. Pasqui, Perry J. Pellechia, and Mark D. Smith

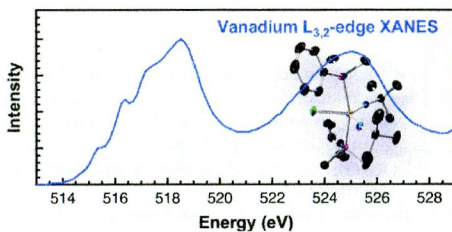
Monohydroxide bridged, dinuclear metallacycles $[\text{M}_2(\mu\text{-OH})(\mu\text{-L})_2](\text{ClO}_4)_3$, $\text{L} = m\text{-}[\text{CH}(\text{pz})_2]_2\text{C}_6\text{H}_4$, $\text{M} = \text{Zn}(\text{II})$ (1); $\text{L} = m\text{-}[\text{CH}(3,5\text{-Me}_2\text{pz})_2]_2\text{C}_6\text{H}_4$, $\text{M} = \text{Zn}(\text{II})$ (2), $\text{Cd}(\text{II})$ (3), have structures in both the solid and solution with a trigonal bipyramidal arrangement about the metals. Complex 1 is fluxional in solution exchanging the axial and equatorial positions of the pyrazolyl rings by a concerted double Berry pseudorotation at both metal sites coupled with the ring flip of the ligand's phenylene spacer by 180° .



Vanadium Bisimide Bonding Investigated by X-ray Crystallography, ^{51}V and ^{13}C Nuclear Magnetic Resonance Spectroscopy, and V $L_{3,2}$ -Edge X-ray Absorption Near-Edge Structure Spectroscopy

Henry S. La Pierre, Stefan G. Minasian, Mark Abubekurov, Stosh A. Kozimor, David K. Shuh, Tolek Tyliyszczak, John Arnold,* Robert G. Bergman,* and F. Dean Toste*

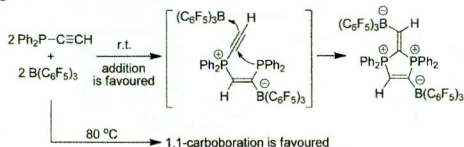
Characterization of vanadium bisimido complexes by X-ray diffraction, ^{13}C NMR, ^{51}V NMR, and V $L_{3,2}$ -edge XANES provides a description of the electronic structure in comparison to group 6 bisimides, group 5 mixed Cp/imide, and group 4 bent metallocene analogues.



Reaction of Diphenylphosphanylacetylene with $\text{RB}(\text{C}_6\text{F}_5)_2$ Reagents: Evidence for a Remarkable Sequence of Synergistic Frustrated Lewis Pair Addition Reactions

Jiangang Yu, Gerald Kehr, Constantin G. Daniliuc, and Gerhard Erker*

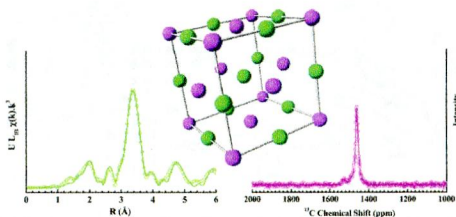
Diphenylphosphinoacetylene and $\text{B}(\text{C}_6\text{F}_5)_3$ undergo a sequence of 1,2-P/B addition reactions to yield a heterocyclic phosphonium/borate-containing dimer.



Coupling XRD, EXAFS, and ^{13}C NMR to Study the Effect of the Carbon Stoichiometry on the Local Structure of $\text{UC}_{1\pm x}$

U. Carvajal Nuñez,* L. Martel, D. Prieur, E. Lopez Honorato, R. Eloiroid, I. Farnan, T. Vitova, and J. Somers

Coupling XRD, NMR, and EXAFS is a powerful means to provide a detailed unambiguous assignment of local structure. The structure of $\text{UC}_{1\pm x}$ was thus accurately assessed, and the effect of the nonstoichiometry was discussed. It was notably shown that the two detected C environments could be attributed to a majority of C atoms in octahedral sites and to the presence of C in interstitial positions.



Pressure Induced Crossover between a Ferromagnetic and a Canted Antiferromagnetic State for [Bis(pentamethylcyclopentadienyl)-iron(III)]Tetracyanoethenide, [FeCp₂]⁺[TCNE]

Jack G. DaSilva, Rodolphe Cl  rac, and Joel S. Miller*

The temperature dependent magnetization for [FeCp₂]⁺[TCNE] is typical of a ferromagnet at ambient pressure but exhibited an extreme reduction with increasing applied pressure, while metamagnetic-like behavior was evident in the field dependent magnetization data at 4.2 kbar.

